Microbes and Mg: Investigating Stable Mg Isotope Fractionation in Microbally Mediated Carbonates

---

A Thesis Presented to

the Faculty of the Department of Earth and Atmospheric Sciences

University of Houston

In Partial Fulfillment

of the Requirements for the Degree

Master of Science

By

Thomas C. Gabel

December 2015

Microbes and Mg: Investigating Stable Mg Isotope Fractionation in Microbally Mediated Carbonates

---

Thomas C. Gabel

APPROVED:

Dr. Henry Chafetz, Advisor

Dr. Thomas Lapen

Dr. Sean Guidry

Dean, College of Natural Sciences and Mathematics

Microbes and Mg: Investigating Stable Mg Isotope Fractionation in Microbially Mediated Carbonates

---

An Abstract of a Thesis

Presented to

The Faculty of the Department of Earth and Atmospheric Sciences

University of Houston

In Partial Fulfillment

of the Requirement of the Degree

Master of Science

By

Thomas C. Gabel

December 2015

Abstract

Microbially induced precipitation is a phenomenon in which minerals are precipitated as a byproduct of the metabolic processes and organic presence (e.g., biofilms) of microorganisms. Commonly responsible are consortia of eubacteria, archaebacteria, and fungi collaborating to complement each other's metabolisms, exchange genetic material, and form the biofilms in which they live. The mineralized remains of these communities have been associated with carbonates in marine or lacustrine settings and, in addition, microbes have been either observed or suggested to be involved in the creation of speleothems, travertine deposits, various carbonate grains (e.g., ooids), and cements.

Magnesium isotope compositions of carbonate minerals are sensitive to the mechanisms of carbonate mineral formation and diagenesis, Mg cycling, and environmental conditions. Data from laboratory experiments suggest that Mg isotope fractionations are dependent on precipitation rates and/or temperature. However, little work has been done to determine whether the information gleaned from sterile, abiotic precipitation experiments are valid if the magnesium bearing minerals are biotically induced.

Calcite was precipitated in free drift experiments, conducted at 25 °C with Mg/Ca molar ratios between 0.2 and 5.6. Data from this study suggests that microbial activity during calcite precipitation influences Mg isotope fractionation in anaerobic environments. The calcite precipitated under these conditions was found to be enriched in ^{26}Mg relative to calcite grown under anaerobic/sterile conditions as well as aerobic

experiments with and without microorganisms. Further inferences were hampered by nonsystematic shifts in isotope measurements introduced by unresolvable organic materials associated with the Mg purification process, and possibly the culture media.

Table of Contents

List of Figures

List of Tables

Chapter 1 - INTRODUCTION

Research on magnesium isotope fractionation in carbonate minerals has focused primarily on samples synthesized in carefully controlled laboratory environments, free of organic influences or biominerals grown by organisms as tests, shells, or skeletal components (Chang et al., 2004; Pogge von Strandmann, 2008; Hippler et al., 2009; Wombacher et al., 2011; Li et al., 2012; Saulnier et al., 2012; Mavromatis et al., 2013). Both growth conditions give insight into the influence of abiotic and biochemical processes on magnesium isotope fractionation, however, the precipitation of naturally occurring carbonate materials commonly takes place in the presence of microorganisms and the byproducts of their life processes. Both living and dead microorganisms and their byproducts have been shown to induce mineral growth through a process known as microbially induced precipitation (Morita, 1980; Buczynski and Chafetz, 1991). In light of this, samples were grown both in the presence and absence of live microorganisms in order to discern the capacity of microbially induced precipitation to affect the fractionation of magnesium isotopes into carbonate minerals.

Bacteria are known to induce mineralization by accentuating the prevailing chemical conditions present to allow for mineral precipitation. This may be done by altering the ambient chemical conditions, e.g., raising or lowering the pH, changing the availability of some ionic species, or water concentration within biofilms (Dupraz et al., 2009). In turn, these manipulations may act in concert with the surface charges exhibited by bacteria along with the extracellular polymeric substances (EPS) generated by colonies as a component of their biofilms (Morita, 1980; Dupraz et al., 2009). The former

process acts by attracting ions to the bacteria's surface and binding them, allowing for the cell membrane to function as a nucleation site which has been observed as a site of mineralization (Morita, 1980, Dupraz et al., 2009). The metabolic activity of a colony along with the dynamic chemical environment within biofilms may also influence how magnesium isotopes are partitioned between the various mineral phases and the surrounding reservoir.

The processes contributing to indirect precipitation of minerals are known collectively as "biotically induced precipitation". These processes act to enhance physiochemical precipitation as a byproduct of the metabolic processes of singular bacterium or the combined efforts of one or more colonies. This differs from the active and intentional mineralization found in organisms such as clams or foraminifera in which energy is expended expressly for the purpose of mineral precipitation. The creation of a mineralized skeleton, test or shell is known as "biomineralizaton" (Dupraz et al., 2009). This distinction of unintentional versus intentional is key in understanding the differing controls affecting mineralization. Thus, microbially induced precipitation will result from a combination of microbial activity and the prevailing chemical environment whereas "biominerals" will reflect the desired results and biases of a mineralizing organism (Dupraz et al., 2009).

For this study, conditions favoring precipitation of polymorphs of calcium carbonate were chosen. Similar conditions with elevated alkalinity and substantial concentrations of calcium and magnesium are not uncommon in nature, and may result in the precipitation of calcite or aragonite, although other mineralogies also occur. Whereas calcium carbonate may be easily precipitated abiotically in the laboratory,

microorganisms may raise the saturation state (Ω) of a solution through reactions that bolster calcite precipitation including the oxidation of carbon and organic nitrogen compounds by aerobic or anaerobic means, the reduction of $CaSO_4$ to CaS by sulfate reducing bacteria, the hydrolysis of urea to form $(NH_4)_2CO_3$, and the uptake of CO_2 by photosynthetic bacteria (Ehrlich, 2002).

The surfaces of bacterial cell membranes are also known to carry an inherently negative charge, which in turn assists in the attraction and binding of calcium and magnesium ions to the surface of the cell (Morita, 1980; Westall et al., 2000; Dupraz et al., 2009, Bundeleva et al., 2012). As a result of this binding process, calcite nucleation is able to occur at lower overall saturation states in the ambient media then in straight physiochemical reactions (Morita, 1980). In response to this phenomenon, many bacteria have evolved means to alter their surface charge through activates such as proton export (Martinez et al., 2008). In some cases, this allows preventing their potential entombment by precipitates, whereas in others, it is part of a complex process of attracting desired nutrients that may inadvertently come at the cost of some amount of calcification (Martinez et al., 2008). Additionally, mineralization of cell membranes, sheaths, and extracellular polymeric substances (EPS) of microorganisms may take place in the absence or presence of live microorganism, however, their degradation by heterotrophic bacteria greatly amplifies the mineralization that results (Chafetz and Buczynski, 1992; Bundeleva et al., 2012).

Biofilms serve as a haven for multitudes of bacteria, improving the efficiency of interactions between cells, allowing for cycling of nutrients, and exchange of genetic information (Westall et al., 2000; Dupraz et al., 2009). The mass of gelatinous

extracellular material surrounding cells, otherwise known as EPS, consists of high molecular weight polysaccharides and plays an important part in the mineralization of microbial mats (Westall et al., 2000; Dupraz et al., 2009). Functional groups within the EPS work to inhibit calcite precipitation by chelating calcium and magnesium ions. This effect is complimented by sequential deprotonation of different functional groups in order to protect against mineralization over a range of pH's (Dupraz et al., 2009). To remove this safeguard and mineralize the EPS, it is necessary that the binding capacity of these functional groups be overwhelmed; this may be achieved via several scenarios (Dupraz et al., 2009).

The first scenario involves the local chemical environment possessing an excess of cations sufficient to saturate the available functional groups. The concentration of cations necessary for this to occur depends on the available functional groups at a given pH, sans losses in binding capacity from intermolecular effects; e.g., steric inhibition (Dupraz et al., 2009). Alternatively, degradation of the EPS, for instance by heterotrophic bacteria, can result in a sufficient spike in cation concentrations to achieve the aforementioned state (Dupraz et al., 2009). Due to spatial and temporal variation in the amount and type of bacteria interacting with the EPS, this latter method will give rise to a corresponding heterogeneity within the biofilm (Dupraz et al., 2009). Therefore, unlike the first scenario, a sufficient saturation state is required to achieve precipitation and may be a localized phenomenon within the biofilm. Mineralization of the EPS also requires suitable alkalinity, supplied either by the surrounding solution or by the bacteria within the biofilm (Dupraz et al., 2009). The latter may be related to bacteria metabolizing the EPS.

Coprecipitation of $MgCO_3$

Magnesium carbonate is commonly found in solid solution with polymorphs of calcium carbonate. This occurs in cases where Mg would otherwise be soluble, but is brought out of solution as Mg substitutes for the major ions of an insoluble carrier phase (inclusion) or adheres to the surface of a growing crystal and eventually entombed within it (surface adsorption and occlusion, respectively) (MARLAP, 2004). Calcite possesses a lattice that is isostructural with that of magnesite ($MgCO_3$), and may incorporate Mg with relative ease (Morse and Mackenzie, 1990). Minor amounts of Mg may be incorporated into aragonite; however aragonite has an orthorhombic crystal lattice that tends to prefer incorporating cations larger than Ca such as Sr over Mg. There is a concern that the Mg found in aragonite samples exists as occluded ions, not incorporated into the lattice of the crystal (Li et al., 2012, personal communication with A. Immenhauser, 2012). Consequently, a sample with Mg adsorbed onto the surface of the aragonite crystal or entombed within it may not be representative of the actual magnesium partition coefficient ($D_{Mg} = [Mg/Ca]_{solid}/[Mg/Ca]_{solution}$) or fractionation factor for aragonite (Morse and Mackenzie, 1990; Li et al., 2012).

In abiotic marine calcite, magnesium carbonate commonly comprises at least 4 mole % of the mineral, averaging approximately 12 mole % and with some biogenic specimens reported as being up to 30 mole % (Morse and Mackenzie, 1990; Wombacher et al., 2011). This is not the case with many terrestrial examples, e.g., speleothems, travertines, and other fresh water carbonate deposits which are, more commonly, low magnesium calcite (LMC), consisting of less than 4 mole % $MgCO_3$. The variation among natural samples may be explained to some extent by the Mg/Ca ratios of the initial

aqueous solution. The average composition of seawater has approximately 3 times as much Mg as Ca; estimates of the average composition of river waters have placed the proportion of Mg as being much lower, however surface and ground water compositions are quite varied both temporally and spatially (Hem, 1985). However, this ratio alone has been found to serve more as an upper limit to Mg incorporation, i.e., calcite produced from solution with a low Mg/Ca ratio will be limited to lower proportions of incorporated $MgCO_3$, and does little in the way of explaining the wide variation found in marine calcites (Given and Wilkinson, 1985).

Efforts to clarify the variation found within laboratory and natural samples have found that in addition to the Mg/Ca ratio, temperature, the ionic strength of the solution, and the kinetics of the precipitation reaction itself exert a control on both how much magnesium is incorporated into the calcite lattice and the stable phases present, i.e., calcite vs aragonite (Given and Wilkinson, Chafetz et al., 1991; 1985; Morse et al., 1997; Zuddas and Mucci, 1998; Watson, 2004; Stephenson, 2011). Observations of the Mg content and $CaCO_3$ mineralogy of recent marine sediments suggests their distribution is strongly affected by the temperature of the sea water from which they precipitate (Morse et al., 1997). Aragonite and high magnesium calcite (HMC) are most commonly found in warm shallow water environments associated with low latitudes, whereas LMC are associated with precipitates formed in colder waters found at greater depths or higher latitudes (Morse et al., 1997). Precipitation experiments on solutions approaching marine salinity were conducted with steady saturation states and temperatures have yielded stability fields as a function of temperature over a range of Mg/Ca ratios that corroborate well with observations of marine examples (Morse et al., 1997). Aragonite was found to

be favored by higher Mg/Ca ratios and temperatures whereas the inverse was true of calcite. For solutions with Mg/Ca ratios lower than 1:5 (e.g., ratios that might be found in fresh waters) the effects of temperature upon mineralogy appear to drop off (Morse et al., 1997).

Ionic strength has been demonstrated to influence both carbonate precipitation rates as well as magnesium partition coefficients in calcite, which has led to some difficulty in comparing results across experiments. The magnesium content of calcite has been found to be not only dependent on ionic strength, but also responds differently to different salts. Magnesium has been found to favor different crystal lattice kink site geometries; ionic strength has been proposed to influence the development of sites in which Mg may be favorably incorporated (Zuddas and Mucci, 1998). Additionally decreases in Mg have been associated with increasing concentrations of NaCl or KCl salts in solutions from which calcite precipitates, this observation has been suggested to be the result of these ions temporarily blocking kink sites on the surface of a growing calcite crystal that might otherwise be preferred by Mg (Stephenson et al., 2011). As hydrated Mg ions are much less readily dehydrated than Ca, the probability of Mg being attached to an unoccupied site and incorporated is thus lessened (Stephenson et al., 2011).

Finally, the kinetics of calcium carbonate precipitation has been shown to influence Mg incorporation. Increased levels of Mg incorporation into calcite have long been associated with more rapid precipitation. Some authors have attributed this effect to a byproduct of a more rapid growth in directions parallel to the c-axis. Calcite crystals consist of layers of Ca and CO_3 ions alternating along the length of the c-axis. Growth in directions parallel to the c-axis continues the pattern of alternating Ca and CO_3 layers.

Precipitation in this manner allows for the incorporation of ions that are not fully dehydrated, lessening the inhibition to growth that results from the dehydration of solvated ions. On these surfaces, the difficulty of dehydrating Mg ions is lessened and with increased rates of growth, Mg ions are buried faster than they might be expelled (Given and Wilkinson, 1985). Alternatively, the growth entrapment model developed by Watson (2004) suggests that the increase in Mg incorporation may be a result of structural and compositional differences between a monomolecular growth layer and the bulk crystal lattice. During incorporation of the new layer into the bulk crystal, diffusion of impurities out of the lattice occurs. The rate at which new layers enriched with Mg can be added verses the rate at which Mg can be removed governs the bulk composition of the resulting crystal (Watson, 2004).

Mg isotopes in carbonates

Isotope fractionation is classified into two broad categories and then into further subcategories. The first are mass dependent fractionation processes, these are instances in which there exists a consistent relationship between the degree of separation and incremental increases in mass. The subcategories of mass dependent fractionation are equilibrium fractionation and kinetic fractionation. The former operates under conditions where a system is closed, under thermal dynamic equilibrium and forward and reverse reaction rates are equivalent. This may be represented by the fractionation of oxygen and hydrogen isotopes within a sealed container of pure water at a constant temperature and pressure. Under these conditions, a consistent proportion of the various oxygen and hydrogen isotopes would develop in each of the phases present. The latter considers

situations in which the forward and reverse reaction rates are not equivalent, in situations where the supply of reactants dictates the rate of reaction or in a system in which the phases present are unable to achieve equilibrium conditions. For example, if the same container of water was exposed to the atmosphere and the vapor produced is allowed to escape, the isotopic composition of the liquid and vapor phases would evolve over time thus, experiencing a form of kinetic fractionation (paraphrased from Kendall and McDonnell, 1998).

The second division is appropriately referred to as mass independent fractionation, i.e., fractionation in which the mass of an isotope has no bearing on its behavior. Fractionation of this manner may be attributed to photochemical reactions or spin-forbidden reactions. The most commonly mentioned examples are the fractionation of oxygen isotopes during ozone formation and sulfur fractionation associated with an atmosphere deficient in oxygen (Heidenreich and Thiemens., 1986; Farquhar et al., 2000).

Studying the fractionation of isotopes within various geological systems has proven to be a powerful tool in gleaning information that complements existing data or provides insight that would otherwise be unobtainable. Well known isotope fractionation systems, such as those of O, C, and S have become pervasive, finding their way into fields such as climatology, petrology, organic chemistry. With the advent of MC-ICPMS, increases in analytical precision make it possible to study elements once thought too heavy to be useful. The stable isotopes of magnesium are promising candidates, however little work has been done to establish a baseline for systems involving microbally induced precipitates.

Nomenclature

In carbonate studies, the ratio of ^{26}Mg or ^{25}Mg to ^{24}Mg are typically reported using the standard delta notation:

$$\delta^{x}\mathrm{Mg} = \left(\frac{(^{x}\mathrm{Mg}/^{24}\mathrm{Mg})_{\mathrm{sample}}}{(^{x}\mathrm{Mg}/^{24}\mathrm{Mg})_{\mathrm{standard}}} - 1\right) \times 1000 \qquad [1]$$

In this equation "x" is either 25 or 26 (Saenger and Wang, 2014). Older or commonly cosmochemistry, literature may instead use $^{x}\Delta$ to report the per mil deviation from a standard (Young and Galy, 2004). These values are usually reported relative to either SRM 980 Mg metal standard or DSM3. Additional standards include seawater, the new NIST solution standard SRM 3131a, created to replace SRM 980, and various mineral standards (e.g., JDo-1 : Dolomite) (Wombacher et al., 2009; Saenger and Wang, 2014). SRM 3131a was created in response to reports that SRM 980 was shown to be heterogeneous (Galy et al., 2003).

The fractionation factor between carbonate minerals and the solutions they are precipitated from is also expressed in the standard notation:

$$\alpha_{\mathrm{carb-sol}} = \frac{(^{x}\mathrm{Mg}/^{24}\mathrm{Mg})_{\mathrm{carb}}}{(^{x}\mathrm{Mg}/^{24}\mathrm{Mg})_{\mathrm{solution}}} \qquad [2]$$

Again, "x" may be either 25 or 26 (Saenger and Wang, 2014). As the fractionation factor is often quite close to unity, the fractionation between carbonate minerals and their associated solutions is commonly reported using capital delta:

$$\Delta^{26}Mg_{carb\text{-}sol} = \delta^{26}Mg_{carbonate} - \delta^{26}Mg_{solution} \quad [3]$$

Three isotope plots comparing $\delta^{25}Mg$ and $\delta^{26}Mg$ are commonly used to assess whether equilibrium or kinetic isotope fractionation has occurred. Assuming the partitioning of ^{24}Mg, ^{25}Mg, and ^{26}Mg differs for equilibrium and kinetic processes, the value of ß in the equation relating $\alpha_{carb\text{-}sol}$ for $^{25}Mg/^{24}Mg$ and $^{26}Mg/^{24}Mg$:

$$\alpha_{25/24} = (\alpha_{26/24})^{ß} \quad [4]$$

[3]

should differ as well (see Young and Galy, 2004 for a derivation of eq. 4) (Young and Galy, 2004). Empirically derived values for ß using three isotope plots can be compared to ß values predicted by stable isotope theory to suggest whether equilibrium or kinetic isotope fractionation has taken place. For Mg equilibrium and kinetic processes ß equals 0.521 and 0.511, respectively (Young and Galy, 2004).

In addition to the typical three isotope diagram, plots of $\Delta^{25}Mg'$ vs $\delta^{26}Mg'$ are often used in order to magnify differences that may not be apparent with traditional three isotope plots (fig. 1). $\Delta^{25}Mg'$ is defined as:

$$\Delta^{25}Mg' = \delta^{25}Mg' - 0.521 * \delta^{26}Mg' \quad [5]$$

[3]

Where $\delta^{25}Mg'$ and $\delta^{26}Mg'$ are defined as:

$$\delta^{x}Mg' = \ln\left(\frac{(^{x}Mg/^{24}Mg)_{sample}}{(^{x}Mg/^{24}Mg)^{standard}}\right)10^{3} \quad [6]$$

[3]

In equation 5, 0.521 corresponds to the ß value for equilibrium fractionation at elevated temperatures. When fractionation occurs under equilibrium conditions, $\Delta^{25}Mg'$ is zero and plots along the equilibrium path, whereas kinetic mass fractionation will land along its own path (fig. 1) (Young and Galy, 2004).

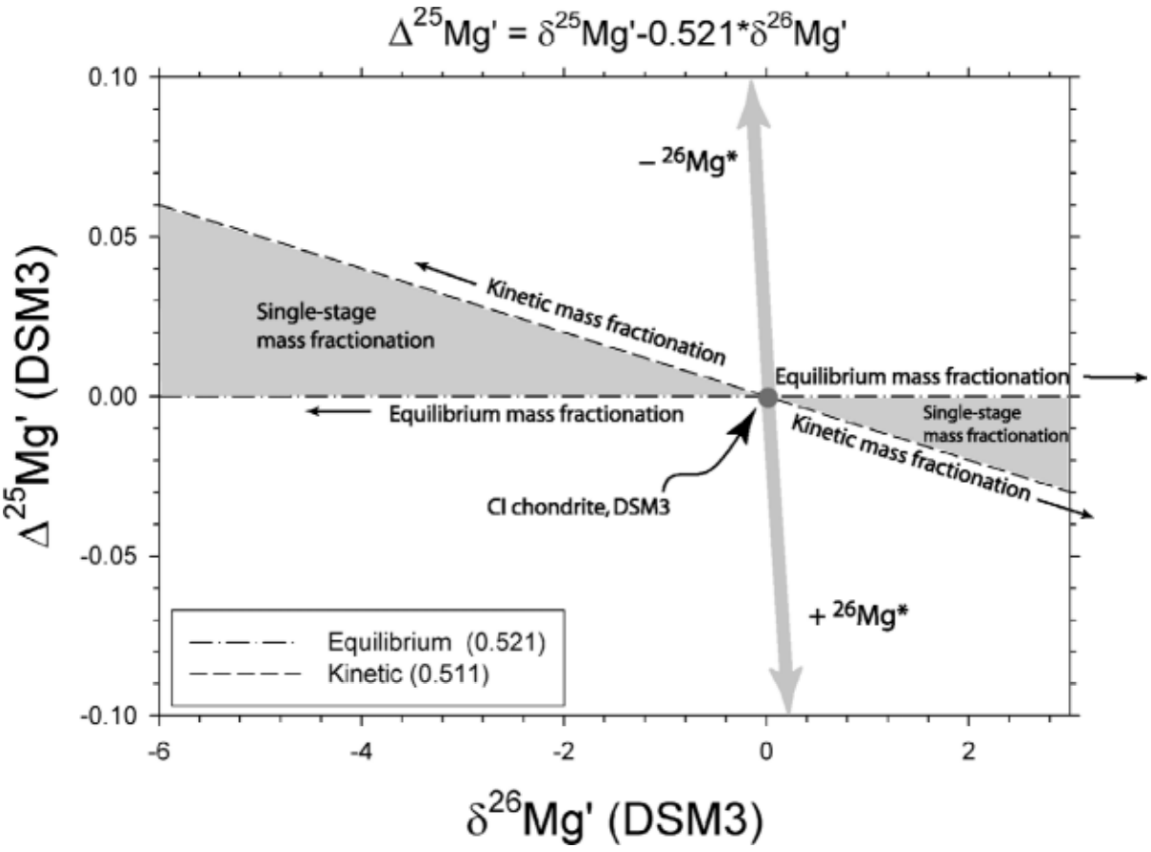

Figure 1. Example plot of $\Delta^{25}Mg'$ (DSM3) vs $\delta^{26}Mg'$ (DSM3). Samples experiencing equilibrium mass fractionation will plot as a line with a slope of zero as $\delta^{26}Mg'$ increases (values given are relative to the DSM3 standard, see Galy et al., 2003). Pure kinetic isotope fractionation will plot along the kinetic mass fractionation line. Grey areas are those reachable by both single and compound events, whereas the white regions require compound events (after Young and Galy, 2004).

Natural Mg isotope variations

Bulk measurement of marine carbonates have found values for $\delta^{26}Mg$ ranging from -5.3‰ to -1‰ (relative to DSM3), in which ^{26}Mg is depleted when compared to the -0.82‰ value found for modern seawater. Studies on biogenic calcite have shown that a similar range of fractionation exists, and differs greatly between species as the result of so called "vital effects". Abiotic precipitation has yielded slightly narrower ranges between parent solutions and calcite, with $\Delta^{26}Mg_{calcite\text{-}solution}$ existing somewhere between -3.16‰ to -1.33‰ across a variety of experimental conditions (Immenhauser et al., 2010; Saulnier et al., 2012; Li et al., 2012; Mavromatis et al., 2013). Insight into abiotic fractionation has been gained from examining fractionation between speleothems and drip water along with a series of laboratory precipitation reactions. Data indicates, thus far, that the isotopic composition of carbonates may differ with mineralogy, be slightly sensitive to temperature, and may experience kinetic effects associated with dehydration of magnesium ions and the rate at which calcite is precipitated (Galy et al., 2002; Immenhauser et al., 2010; Li et al., 2012; Saulnier et al., 2012; Mavromatis et al, 2013; Wang et al., 2013a).

Role of mineralogy

Different carbonate minerals appear to experience different fractionations. It has been suggested that carbonates will deviate from their starting solution in the order: aragonite < dolomite < magnesite < calcite. Wang et al. (2013a) explains that this is a function of the strength of the Mg-O bonds binding magnesium. The length of the Mg-O bonds increases in a similar fashion: aragonite (2.08 Å) = dolomite (2.08Å) < magnesite

(2.105Å) < calcite (2.12Å), where longer bonds are associated with weaker bonds. Aragonite has a similar bond length to dolomite; however, it has a higher 9-fold coordination than its peers, who have 6-fold coordination (fig. 2) (Wang et al., 2003a). The stronger the Mg-O bond, the more likely ^{26}Mg will be incorporated into the mineral lattice (Saenger and Wang, 2014).

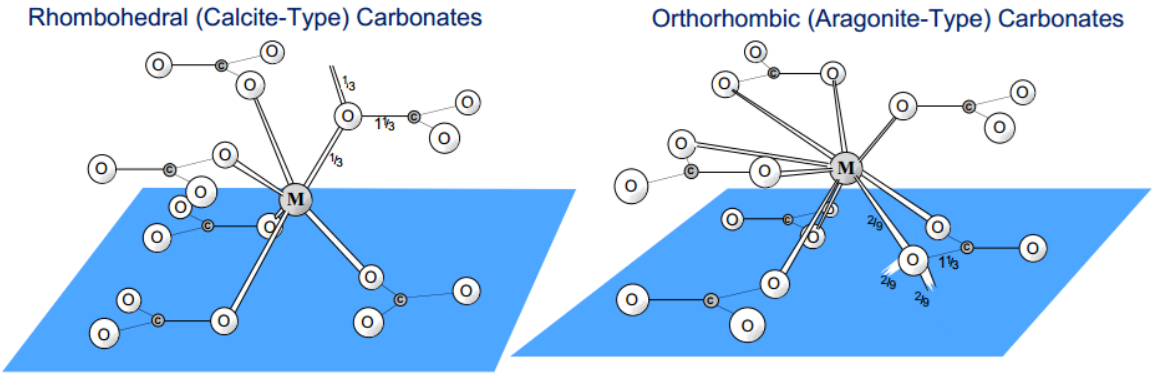

Figure 2. Calcite 6-fold coordination, aragonite 9-fold coordination (after Railsback, 2006)

Another possibility may reside in the surface properties of the minerals. Wombacher et al. (2011) suggests that incorporation of cations at kink sites (fig. 3) on the growing mineral's surface requires both the dehydration of the attachment site and the cation. If differences in the surface properties of the various minerals are sufficient to alter the activation energy necessary to bond magnesium, a mineral specific fractionation may result (Wombacher et al., 2011).

Role of temperature

Temperature dependence has been reported for both abiotic calcite and aragonite studies. Li et al. (2012) conducted free drift experiments using magnesium free seed crystals at temperatures between 4°C and 45°C. The data show that with each 1C °

increase of temperature, Δ^{26}Mg approaches closer to zero by 0.011±0.002‰ (Li et al., 2012). Wang et al. (2013a) found a similar trend in aragonite (0.009±0.001‰ $°C^{-1}$) using free drift experiments at temperatures between 35 °C and 55 °C. Other abiotic precipitation experiments with calcite do not reflect this trend (fig. 4) and display trends unrelated to temperature (Immenhauser et al., 2010; Saulnier et al., 2012; Mavromatis et al., 2013).

Additionally, Saenger and Wang (2014) note that due to an external precision of approximately 0.1‰, the temperature sensitivity of calcite (approximately 0.01‰ $°C^{-1}$) requires a minimum change in temperature of 10 °C for a difference in temperature during precipitation to be discernable. It is suggested then that the application of magnesium in carbonates is currently limited to large shifts in temperature, at least until analytical precision improves (Saenger and Wang, 2014). Furthermore, as it would appear, temperature dependence is not a consistent phenomenon, at least in calcite, the utility of magnesium isotopes for temperature determinations is dubious.

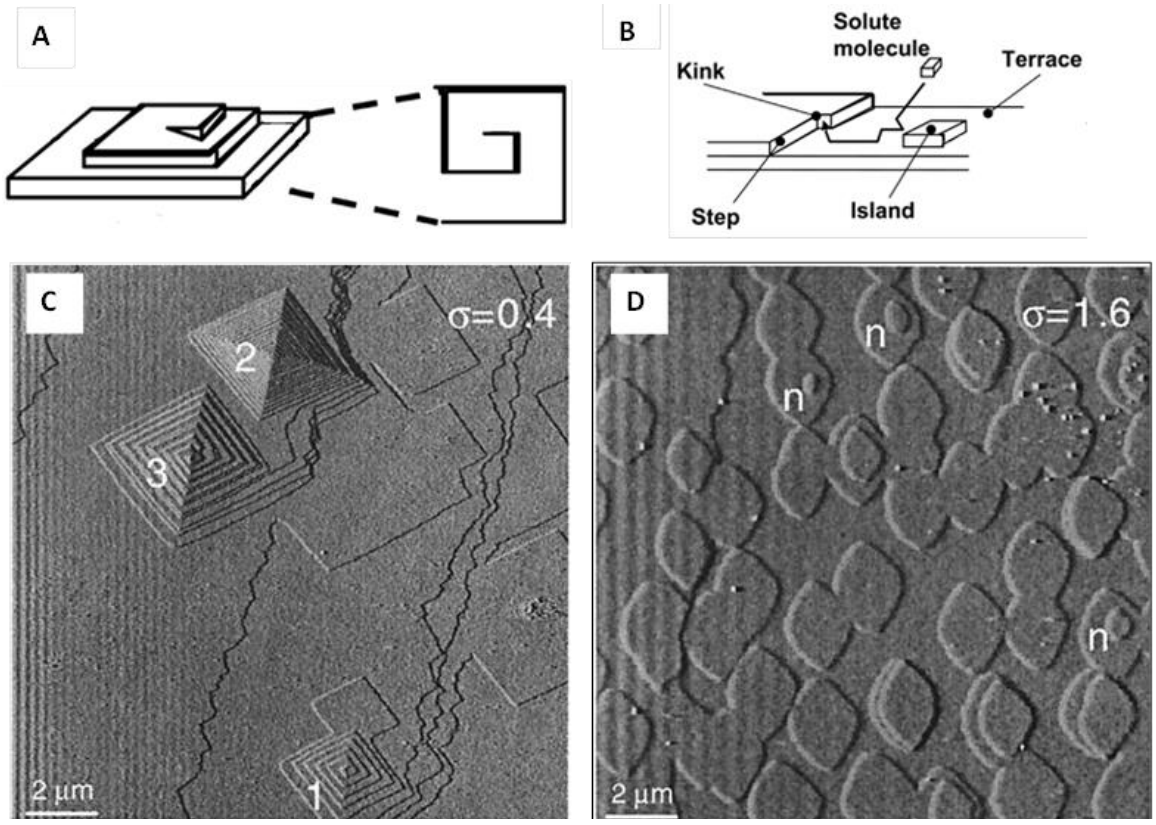

Figure 3. Two dimensional and spiral growth in calcite. (A) and (B) Schematic diagrams of spiral and two dimensional growth, respectively (modified from De Yoreo and Vekilov, 2003). (C) and (D) AFM images of spiral growth taking place at low saturation and two dimensional growth taking place at higher saturation states. Here lower case sigma is the saturation state (after Teng et al. 2000).

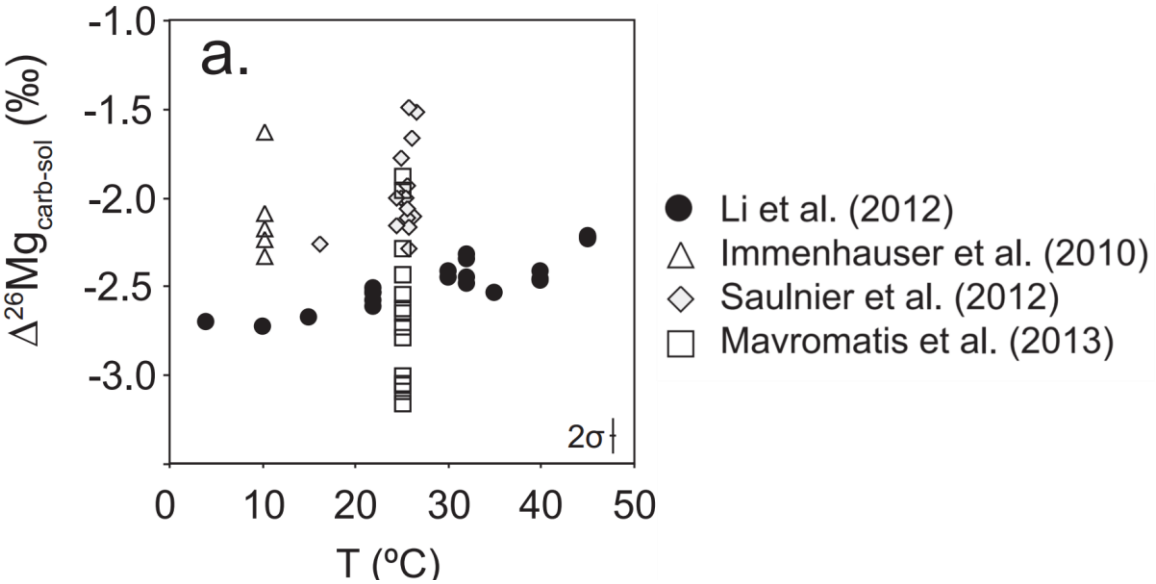

Figure 4. $\Delta^{26}Mg$ vs temperature. Only Li et al. (2012) data points appear to respond systematically to temperature (After Saenger and Wang, 2014).

Role of precipitation rate

Experiments by several researchers show a decrease in magnesium isotope fractionation with increasing precipitation rates that coincides with an increase in the amount of magnesium incorporated into calcite (fig. 5) (Immenhauser et al., 2010; Saulnier et al., 2012; Mavromatis et al., 2013). Immenhauser et al. (2010) and Mavromatis et al. (2013) suggest that this trend is an increase in the partition coefficient for magnesium (D_{Mg}) along with kinetic fractionation, both related in some way to the difficulty in dehydrating magnesium ions. It has long been suggested that the partition coefficient of Mg is related to calcite's growth rate, and the strong hydration of magnesium (Given and Wilkinson, 1985). This is explained as a result of calcite's crystal structure wherein attachment of hydrated ion occurs preferentially on faces perpendicular to the minerals c-axis (fig. 6) or as Immenhauser et al. (2010) and Mavromatis et al. (2013) have suggested as the result of surface entrapment. Watson (2004) proposes a model in which the final composition of a crystal is dependent on inherent differences in the surface composition (both isotopic and chemical) of a crystal and that of the composition of its bulk. Depending on the rate of precipitation versus the rate at which impurities can diffuse out of the crystal, the composition of the surface becomes trapped as it is entombed under subsequent growth (Watson, 2004). Mavromatis et al. (2013) support this assertion with FTIR data showing increases along the 3345 cm^{-1} and 1630 cm^{-1} bands associated with water that coincide with an increase in the mole % $MgCO_3$ in the calcite which is interpreted as an increase in partially hydrated magnesium ions

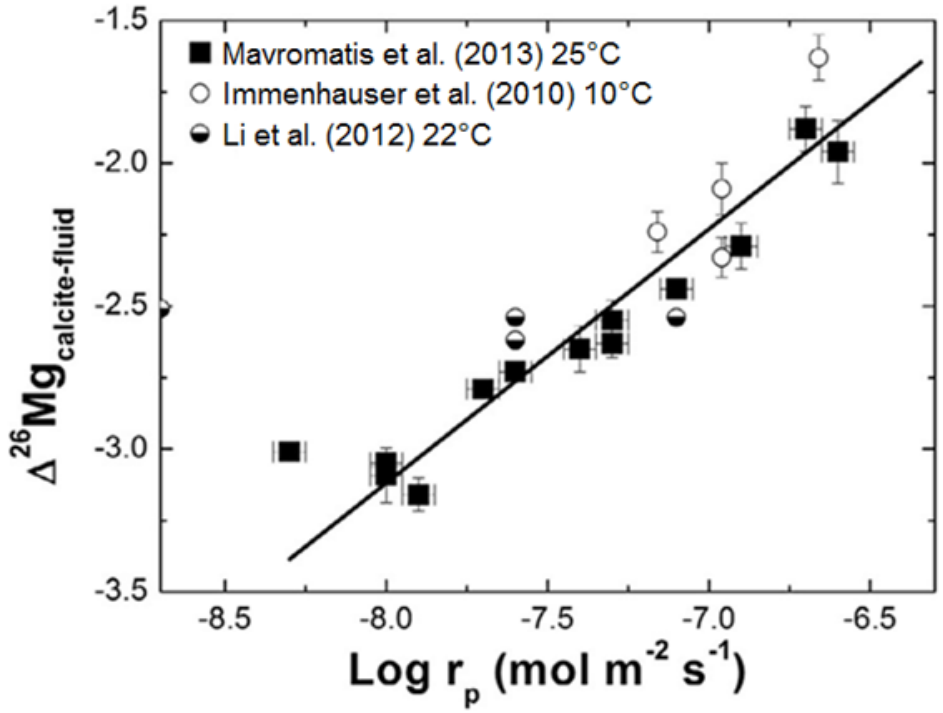

Figure 5. $\Delta^{26}Mg$ vs precipitation rate. Mavromatis et al. (2013) data show that the difference between the bulk calcite and solution $\delta^{26}Mg$ ($\Delta^{26}Mg_{calcite\text{-}fluid}$) decreases linearly with the logarithm of the growth rate of calcite (Log r_p (mol $m^{-2}s^{-1}$)). That is, the amount of Mg isotope fractionation observed is seen to decrease as the rate of calcite growth increases, a trend also found in data from Immenhauser et al. (2010), and Li et al. (2012). (modified from Mavromatis et al., 2013).

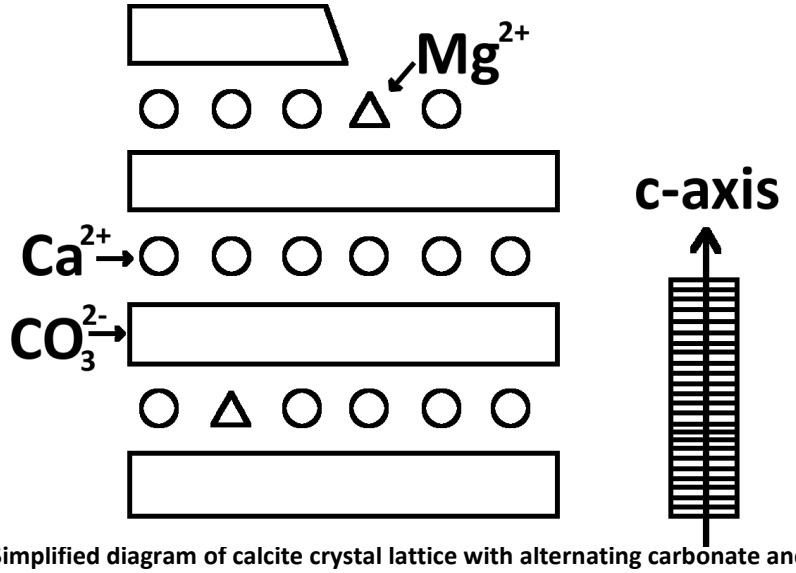

Figure 6. Simplified diagram of calcite crystal lattice with alternating carbonate and calcium layers; incorporation of Mg ions occurs preferentially along planes perpendicular to the c-axis where full dehydration of the Mg ion is not necessary for attachment (Modified from Folk, 1974).

incorporated into the calcite lattice. The idea is that surface entrapment, fractionation related to the dehydration of the hydrated magnesium, along with any other discriminating factors is simply ignored at higher rates of precipitation (Mavromatis et al., 2013)

Saulnier et al. (2012) puts forth an alternative explanation; that the trend of $\delta^{26}Mg_{carb}$ towards the fluid values is the result of much of the magnesium in the calcite existing in fluid inclusions. That is, with faster precipitation, fluid inclusions containing unfractionated aqueous Mg become increasingly abundant. A mixing model created by Saenger and Wang (2014), with one end member set to solution values ($D_{Mg} = 1$; $\Delta^{26}Mg_{calite\text{-}solution} = 0$) and the other to an estimated equilibrium value for D_{Mg} and $\Delta^{26}Mg_{calite\text{-}solution,}$ appears to fit the data of Immenhauser et al. (2010) and Mavromatis et al. (2013) fairly well. Consequently, Saenger and Wang (2014) suggest that up to approximately 1.1% of the Mg in calcite samples from these studies may have been derived from fluid inclusions (Saenger and Wang, 2014). The mixing model does not match perfectly, and many of Li et al. (2012) and Saulnier et al. (2012) data points lie off of the curve.

Temperature vs kinetic effects

Differences in experimental design may have allowed mineral growth through different pathways, Li et al. (2012) and Wang et al. (2013a) precipitated their minerals using free drift experiments and solutions with relatively high saturation states ($\Omega \geq 4.2$), high magnesium concentrations, and Mg/Ca ratios. A rapid increase of saturation state and high Mg/Ca ratio may have allowed precipitation of carbonate minerals through an

amorphous precursor that would then decompose into calcite or aragonite (Saenger and Wang, 2014). The experiments of Mavromatis et al. (2013) and Immenhauser et al. (2010) were conducted under steady state conditions, with lower saturation states ($\Omega \leq 3$), magnesium concentrations, and Mg/Ca ratios that would not have favored the precipitation of amorphous calcium carbonate (Saenger and Wang, 2014). The effects of an amorphous precursor on isotope fractionation are not known at the present, and the use of seed crystals in Li et al. (2012) makes the nucleation of an amorphous phase unlikely (Saenger and Wang, 2014).

The differences in the saturation states of the experiments may have also resulted in different growth patterns during precipitation. At the higher saturation states of Li et al. (2012), two dimensional growth takes place (fig. 3b and d). At lower saturation states spiral growth is favored (fig. 3a and c) (Teng et al., 2000; De Yoreo and Vekilov, 2003). As calcium isotopes have been found to be more sensitive to precipitation rate during spiral growth, it is suggested that magnesium may behave similarly (Nielsen et al., 2012). Mavromatis et al. (2013), with a constant, low saturation state may have experienced only spiral growth and therefore felt more acutely the dependence on precipitation rate (Saenger and Wang, 2014).

Additionally, different Mg/Ca ratios used affect calcite step velocities. Increases in the Mg/Ca ratio correspond with decreasing step velocities up to approximately 1.7 mol/mol, after which the rate at which steps on the mineral's surface (fig. 3b) advance are essentially constant. This is likely associated with Mg blocking kink sites. Lower Mg/Ca ratio experiments may have experienced significant differences in step velocities whereas

those above the threshold remained relatively constant, and therefore would be less influenced by precipitation rate. If this were the case, the subtle temperature dependence would be visible (Saenger and Wang, 2014).

Lastly, different pH ranges in the experiments likely resulted in the distribution of magnesium into various aqueous complexes. Magnesium speciation in aqueous solution may result in either a fractionation between species or an effect on the rate of precipitation (Saenger and Wang, 2014).

Biominerals

δ^{26}Mg values reported for biominerals range from ca. -5‰ to -1‰ and may potentially be explained by mineralogy, temperature dependence, precipitation rate, and the speciation of aqueous magnesium (Li et a;., 2011; Sanger and Wang, 2014). So called "vital effects" produced by the life activities of organisms may further dictate the final fractionation seen.

HMC (high magnesium calcite)

Some organisms that precipitate high magnesium calcite (greater than 4 mole % $MgCO_3$ (Morse & Mackenzie, 1990)) fall along the abiotic temperature dependent trend of Li et al. (2012), presenting possible candidates for paleoclimate data (limited by analytical precision) (Saenger and Wang, 2014). Also, as the magnesium concentration and Mg/Ca ratio of seawater better match those of Li et al. (2012), marine calcite would presumably not favor the dependence on precipitation rate seen by Immenhauser et al., (2010) and Mavromatis et al. (2013).

The use of biomolecules, and in some cases an amorphous calcium carbonate (ACC) precursor may explain the offset seen in some species. Organisms that produce HMC via a ACC precursor have been shown to use biomolecules that preferentially bind Ca, thus raising the Mg/Ca ratio of the solution from which the precursor is precipitated, in this way the Mg/Ca ratio of the resulting calcite may be increased (from 21 to 34 mole % (Raz et al., 2000)). While the fractionation due to the formation of an ACC precursor remains unclear, the biomolecules produced to raise the local Mg/Ca ratio may cause enrichment in ^{26}Mg and ^{44}Ca by preferentially binding the lighter isotopes of each element. This may be an explanation for HMC producing organisms that $\Delta^{26}Mg_{calcite\text{-}solution}$ are less negative than abiotic counterparts (Saenger and Wang, 2014)

LMC (low magnesium calcite)

$\Delta^{26}Mg_{calcite\text{-}solution}$ in organisms producing LMC (less than 4 mole % $MgCO_3$ (Morse & Mackenzie, 1990) is more variable than in HMC calcifiers. The LMC produced by most organisms exhibit little or no dependence on temperature (Saenger and Wang, 2014). The few in which a dependence has been observed, do not match the sign or sensitivity found in abiotic experiments, suggesting temperature to be subordinate to some other process. Precipitation rate may play some role, however its importance is variable across different species. The partition coefficient of magnesium (D_{Mg}) for biotically produced calcite is often much lower that its abiotic counterparts (Saenger and Wang, 2014). Whereas the production of HMC may be enhanced by raising the local Mg/Ca ratio, organisms producing LMC commonly precipitate LMC from isolated reservoirs. By actively removing magnesium or alternatively incorporating magnesium

into organic molecules in order to lower magnesium concentration, the remaining fluid would then become enriched in ^{26}Mg (Saenger and Wang, 2014).

Aragonite

Biogenic aragonite seems to altogether lack the temperature dependence seen in Wang et al., (2013a). This may be the result of improper cleaning techniques leading to additions of magnesium adsorbed to the surface, or contained within the organic materials, or clay minerals embedded in the sample rather than the sample itself and/or a lack of analytical precision that would easily hide aragonite's weak temperature dependence (Wang et al., 2013a).

Biotically Induced Precipitation

Whereas biominerals are the product of biologically controlled mineral precipitation, biotically induced precipitates are formed coincidentally due to the vital activities of an organism (Dupraz et al., 2008). This is most famously exemplified in microbialite deposits (e.g., stromatolites). Here microorganisms can affect mineral precipitation altering the ambient chemical conditions, e.g., raising or lowering the pH, changing the availability of some ionic species, or water concentration within biofilms (Dupraz et al., 2008). In turn, these manipulations may act in concert with the surface charges exhibited by bacteria along with the extracellular polymeric substances (EPS) generated by colonies as a component of their biofilms (Dupraz et al., 2009).

EPS has been shown to chelate cations as part of its function in a biofilm to resist calcification (Dupraz et al., 2009); it may be that this produces an effect similar to the

effect suggested for biomolecules in HMC producing organisms or ion exchange resins (Teng et al. 2007; Saenger and Wang, 2014). Alternatively, variations in precipitation rate may result in any of the kinetic effects reported in Mavromatis et al. (2013).

Current research suggests that the presence of cyanobacteria has little to no effect on Mg isotope fractionation in hydrated magnesian carbonates (Mavromatis et al, 2012; Sirokova et al., 2013). The literature in this area is otherwise nonexistent.

Chapter 2 - METHODS

Field Work

The microorganisms used in this study were collected from the sediment of Lake Livingston, Livingston, TX (fig. 7). Samples were collected with sterilized pipe cleaners that were inserted into the first few centimeters of sediment submerged below the surface of the lake near the shore line. These were then deposited into non-nutritive agar with a water profile approximating the composition of the lake water and then placed on ice

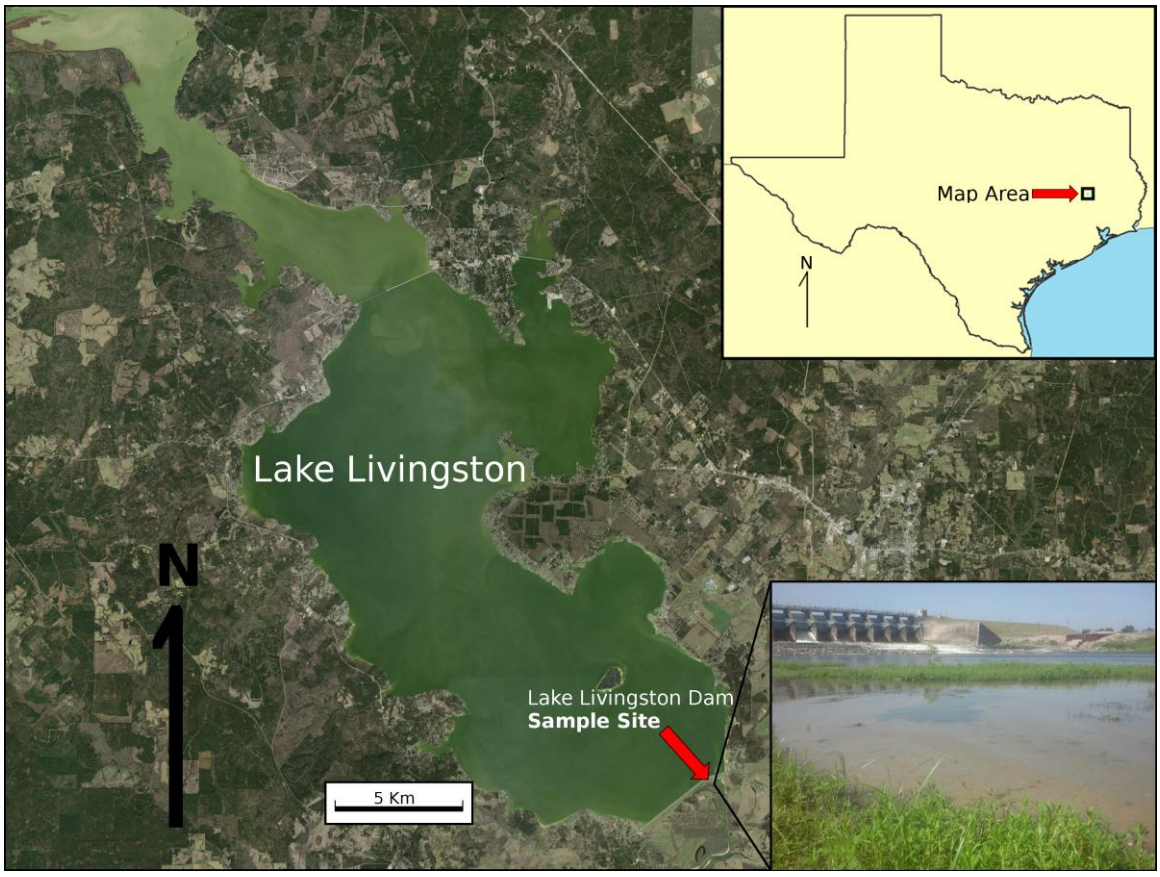

Figure 7. Map of sampling location. Microorganisms used in this study were collected from a pool of water near the base of the Lake Livingston Dam. No calcite precipitation was observed in the sample area coordinates: 30°37'40.27" N, 95°00'42.23" W.

prior to returning to the lab. When samples were taken, duplicate sterile pipe cleaners were removed from the same package and exposed to the air and treated identically. These were later deposited in culture media to determine if contamination had occurred prior to collection from the lake. At each site readings for pH and conductivity were taken.

Culturing

Upon returning to the lab, the inoculated and blank pipe cleaners were deposited into vials of tryptic soy broth (TSB) and allowed to incubate at 25 °C for 48 hours. Successful inoculation was confirmed by the development of a thick haze in the previously clear liquid. Media used with the exposed, but unused pipe cleaners remained clear and unchanged. This suggests the microbes used in this experiment were derived exclusively from the locations from which samples were collected.

Precipitation Experiments

Unbuffered TSB proved to have a pH unsuitable for carbonate precipitation. Instead medium 2216E for anaerobes was selected. This consisted of 5.0 g/l bacto peptone, 0.1 g/l ferric phosphate, 1 liter deionized water substituted for aged sea water (Medium 2216, ZeBell, 1941), 1.0 g/l yeast extract (Medium 2216E, Gunkel and Reinheimer, 1968, as noted in Krumbein, 1971), 5.0 g/l D-glucose and 0.1 g/l L-ascorbic acid (2216E for anaerobes, Krumbein, 1971). To this media, approximately 0.015 - 0.05 M $CaCl_2$ and approximately 0.01 - 0.08 M $MgCl_2$ were added from stock solutions, along with 0.05 M of $NaHCO_3$ powder. Initial attempts to sterilize the media by autoclaving resulted in precipitation of carbonate material. In lieu of autoclaving, one batch was

prepared from sterile ingredients, and later batches were sterilized by vacuum filtration through disposable Corning 500 ml bottle top filtration units with 0.22 μm polyethersulfone membranes (fig. 8b). No visible signs of contamination in vials containing sterile media occurred in either case. With the exception of the initial batch, the deionized water used for culture media was chilled to approximately 4 °C prior to preparation and culture media was kept cold in an ice bath (fig. 8a) throughout preparation, filtration, and just prior to use in order prevent outgassing of CO_2 and early precipitation. Representative samples collected from unused media were tested for the initial pH for each batch and ranged between 7.09-7.6. Additionally, vials of unused media were filled to the brim and stored at approximately 4 °C for later analysis.

Precipitation experiments were carried out in borosilicate glass bottles and vials that were washed with soap, rinsed in deionized water, acid washed in 10 % nitric acid for a period no less than four hours, rinsed with deionized water, and sterilized by autoclaving prior to use. The volume of the vessels ranged between 9.5 drams (approximately 35 ml) and 125 ml.

Each batch consisted of 12-16 media filled containers under aerobic or anaerobic conditions, half of which were left sterile and the other half inoculated with microorganisms cultured from samples taken from the field. Aerobic samples were plugged with sterile cotton plugs to prevent contamination by airborne dust and microorganisms (fig. 8c). Anaerobic samples were filled to overflowing and capped off to prevent additional oxygen from entering the vessel (fig. 8c). When uncapped, inoculated anaerobic samples smelled foul and were often under pressure, effervescing with a

nonflammable, odorless gas that readily came out of solution. This gas was likely CO_2, suggesting that fermentation was taking place and that anaerobic conditions had ensued after any dissolved O_2 present was depleted. All runs were performed at approximately 25°C (fig. 8d) and were allowed to continue for between 1 and 6 months prior to being prepared for analysis. Samples of precipitates were taken after noticeable precipitation had ceased and examined for mineralogy and morphology. The final pH of the culture media was also measured (table 3). A workflow for the above processes can be seen in fig. 9.

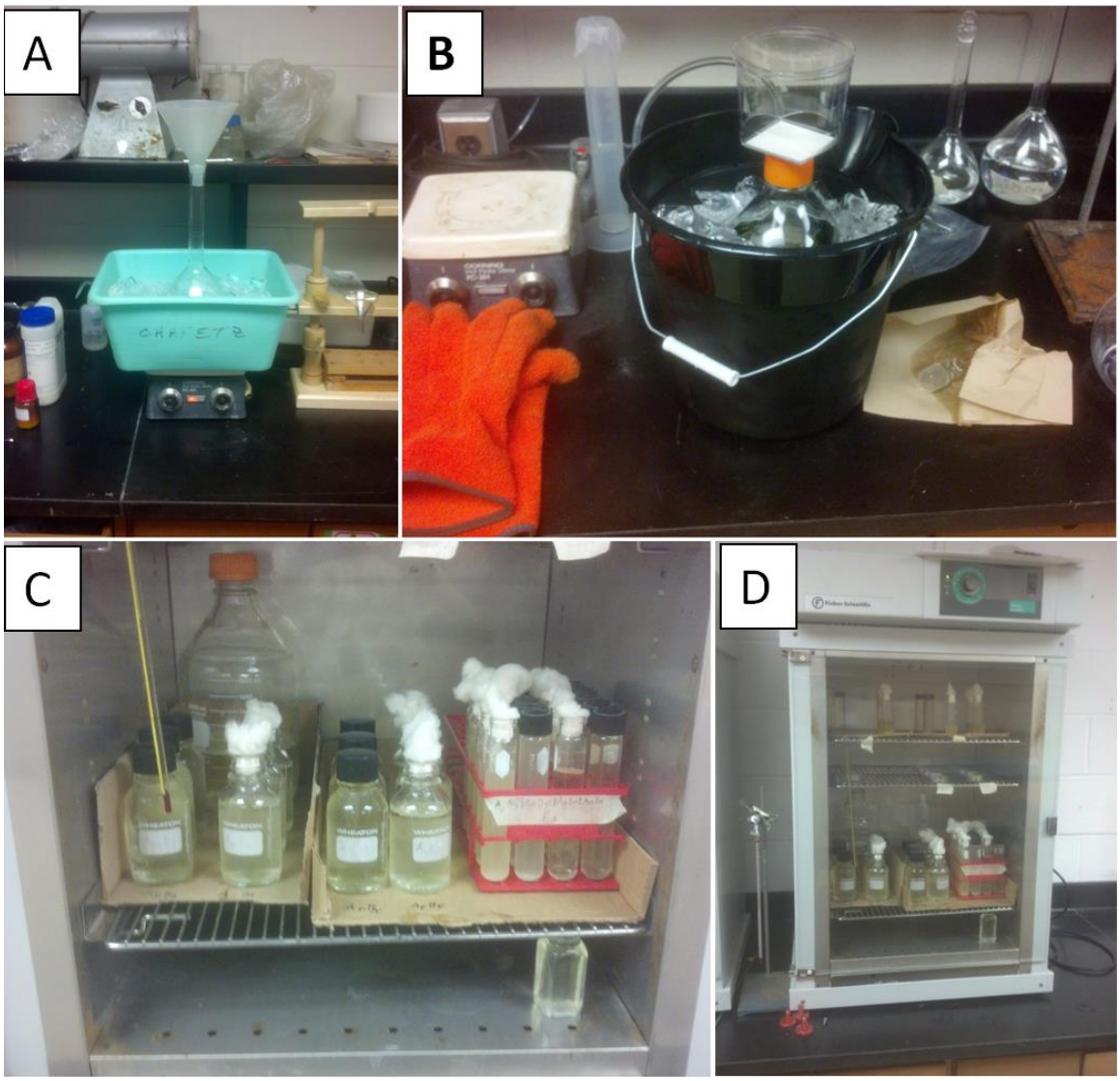

Figure 8. Experimental setup. (A) Culture media kept chilled during mixing, (B) culture media is sterilized by vacuum filtration through a 0.22 µm polyethersulfone membrane and kept chilled by an ice bath to avoid unwanted precipitation, (C) inoculated samples (left) and sterile samples (right) in bottles either capped off or plugged with sterile cotton to prevent contamination, and (D) samples are kept inside a temperature controlled incubator at ~25°C.

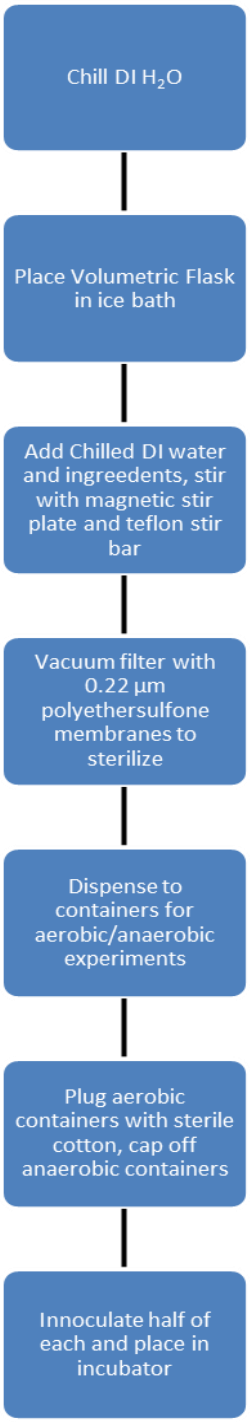

Figure 9. Workflow for culture studies.

Examination of Precipitates

Precipitates were sampled and analyzed for mineralogy with x-ray diffraction on a Siemens D 5000 x-ray diffractometer using a zero back ground holder consisting of an oriented quartz crystal mounted within an aluminum frame. Prior to analysis the precipitates were centrifuged and pipetted and/or scraped from the sides of containers to separate them from the broth media and rinsed in ultrapure water. These were then dried overnight and pulverized into a fine powder with a glass mortar and pestle.

A scanning electron microscope was used for imaging the precipitates. Samples floating on the surface of the broth media were lifted out using a variety of spatulas and other implements. Samples that had grown on or had sunk to the bottom of the containers were either centrifuged and then pipetted or simply pipetted after removing most of the liquid. These were then deposited on graphite disks for imaging.

Purification of Mg for Isotope Analysis

Prior to column chemistry samples were vacuum filtered to separate any precipitates from the liquid media. The filtered precipitates and those that remained within the containers were then rinsed with ultrapure water and set aside. Five milliliters of the liquid growth medium was subsampled for isotope analysis. An addition of 1-5 ml of 30% H_2O_2 was added to each subsample after which they were dried at a low heat (<50°C) in order to oxidize any dissolved organic matter. Often less than 5ml 30% H_2O_2 was required, and temperatures above 50°C were found to produce an excessively vigorous reaction. Both the precipitate and water samples were dissolved in

approximately 6M HCl and dried in savillex Teflon vials, dissolved in HNO_3 to remove any remaining organic material and dried, and finally dissolved again in approximately 6M HCl and dried again prior to preparation for column chemistry, following the initial round of samples, subsequent samples were later fluxed overnight with 2 ml of aqua regia at 130 °C to oxidize the remaining organics, before drying the sample and converting it to chlorides.

Following the removal of organic material and conversion to chloride form, Mg was purified in three steps to remove elements that might otherwise create isobaric interferences (e.g., $^{48}Ca^{2+}$, $^{48}Ti^{2+}$, $^{50}Ti^{2+}$, $^{50}V^{2+}$, $^{50}Cr^{2+}$and$^{52}Cr^{2+}$) and/or affect the instrumental mass discrimination encountered by the sample verses the standard (e.g., Al, Fe, Na, Ni, and Ca) (Young and Galy, 2004; Bizzarro et al., 2011). These steps are as follows:

1. Fe removal: A Bio-Rad 10 ml column was packed with 2.5 ml of Dowex 1x8-200 mesh resin, which was then cleaned with 4 column volumes of approximately 6 M HCl, alternating with 3 column volumes of ultrapure water, and lastly conditioned with one column volume of 6.0 M HCl. The dried samples were first dissolved in 1 ml 6.0 M HCl, then loaded on the column. Mg was eluted with 5 ml of 6.0 M HCl while Fe was retained on the resin. Fe was eluted into a waste container with 2 column volumes of approximately 0.4 M HCl and the resin was cleaned with 1 column volume ultrapure water prior to reuse.
2. Cr, Na, Al, Ti clean up: A section of the method developed by Bizzarro et al. (2011) was slightly modified to include a possibly omitted resin cleaning step.

A Bio-Rad 10 ml column packed with 1 ml of BioRad AG50W-x8 200-400 mesh resin was cleaned with 16 ml of approximately 6 M HCl (2x 8ml), and conditioned with 9 ml of 0.5 M HCl (3x 3 ml). Samples were dissolved in 0.5 ml of 0.5 M HCl and loaded on the column. Chromium and sodium were eluted with 3ml of 0.5 M HCl, followed by 4 ml of 1.0 M HNO3. Aluminum and titanium were eluted with 2 ml of approximately 2M HF. Lastly Mg was eluted with 8 ml of 6.0 HCl and dried before being converted to nitrates and a subsample was diluted in 2% Optima HNO3 for optical emission spectroscopy (OES) to determine the Mg and Ca concentrations. The remaining samples where then dried and converted back to chlorides with approximately 6 M HCl.

3. Ca removal: Calcium was removed using the Mg purification method developed in Wombacher et al. (2009). Columns made of similar materials and dimensions to the pipette columns used by Wombacher et al. (2009) (fig. 10) were packed with 1 ml of Biorad AG50-x8 200-400 mesh resin and cleaned with 30 ml of approximately 4 M HCl. Two milliliters of approximately 10 M HCl were then used to condition the column. Samples were dissolved in 0.25 ml of approximately 10 M HCl and loaded onto the column. Mg was then eluted with 2.5 ml of approximately 10 M HCl. As Ca and Fe were not of interest, the remaining Ca and Fe were eluted into a waste container with another 30 ml of approximately 4 M HCl prior to reuse of the resin. Later the first two columns were replaced by the second stage of Wombacher et al.'s (2009) method.

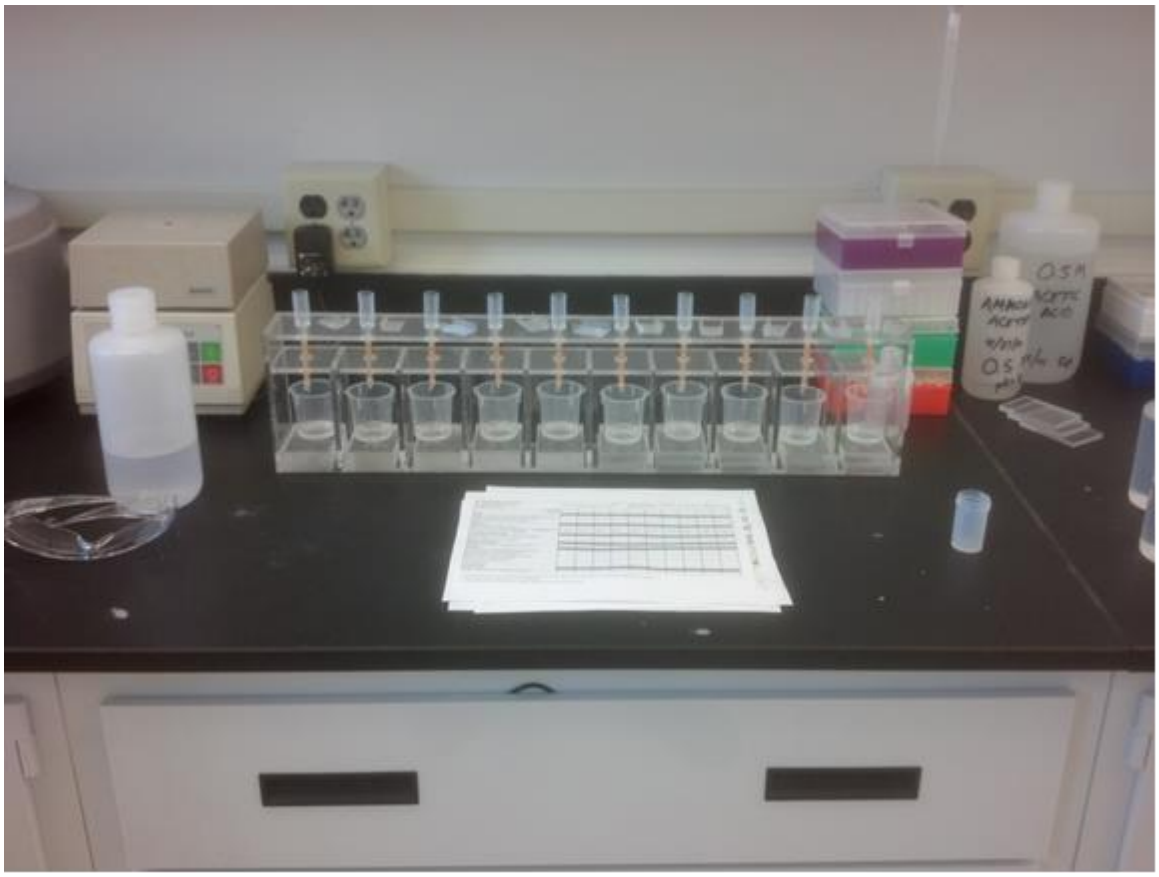

Figure 10. Custom columns made from LDPE transfer pipettes. Pipette dimensions closely match those used in Wombacher et al. (2009). To prevent resin leaks it was necessary to ensure the sides of the frit were aligned parallel to the pipette walls. Heating the tip of the pipette to mold it around the frit was also helpful.

Following stage 1, samples were dried and brought up in 0.4 M HCl. The same columns were conditioned with 11 ml of 0.4 M HCl (5 ml, 3 ml, 3 ml) and the sample was then loaded onto the column. The matrix was then eluted with 28 ml of 0.4 M HCl and Be, Al, and Ti with 6ml of 0.15 M HF. Following a wash with 1 ml of ultrapure H_2O and an addition of 1 ml 1.0 M HCl, Mg was collected with an additional 12 ml of 1.0 M HCl before being dried. Following this samples were brought up in 50 µl of a 50/50 mixture of concentrated HNO_3 and H_2O_2 and dried three times in order to remove residual organic matter and convert the samples to nitrates before being brought up in 2%

Optima HNO_3 for analysis. Column calibrations conducted before and between batches of samples show >99% yield with blanks ranging between 8 and 12 ng of Mg. It is unknown if there is a limit to the number of time the resin may be reused. Following dissolution in 2% Optima HNO_3 and a concentration check, subsamples of 2000 ng/ml Magnesium were analyzed using a standard-sample-standard bracketing technique. Samples were measured and reported relative to standard NBS 980, and were run alongside HPS 909104 and HPS 932001. The isotopic composition of the standards used along with the isotopic composition of the experimental Mg sources and test solutions are presented relative to NBS 980 in table 1. A workflow diagram for the Mg purification process can be seen in fig. 11.

Table 1
Mg isotope composition of standards, Mg sources, and test solutions passed through ion-exchange chromatography. All data are reported relative to NBS 980

Sample	$\delta^{26/24}$Mg	2 SD	$\delta^{25/24}$Mg	2 SD	n
Isotope Standards					
NBS 980	-0.01	0.09	-0.01	0.07	120
HPS 909104	3.30	0.09	1.69	0.05	16
HPS 932001	1.16	0.09	0.60	0.05	17
Reported Isotope Compositions					
HPS 909104 (Li et al, 2012)	3.42	0.13	1.76	0.08	49
HPs 932001 (Li et al. 2012)	1.19	0.13	0.60	0.08	48
Magnesium sources					
0.5 $MgCl_2$*	2.18	0.05	1.09	0.05	1
3 $MgCl_2$**	1.67	0.05	0.84	0.05	1
Test Solutions					
14-247 NBS 980 10,000ng Mg	-0.96	0.11	-0.51	0.01	0.07
14-269 NBS 980 10,000ng Mg	-1.36	0.11	-0.71	0.01	0.07

n: number of analyses. 2 SD: two standard deviations.
* Mg Source (2), (3), (4), (5)
** Mg Source (6)

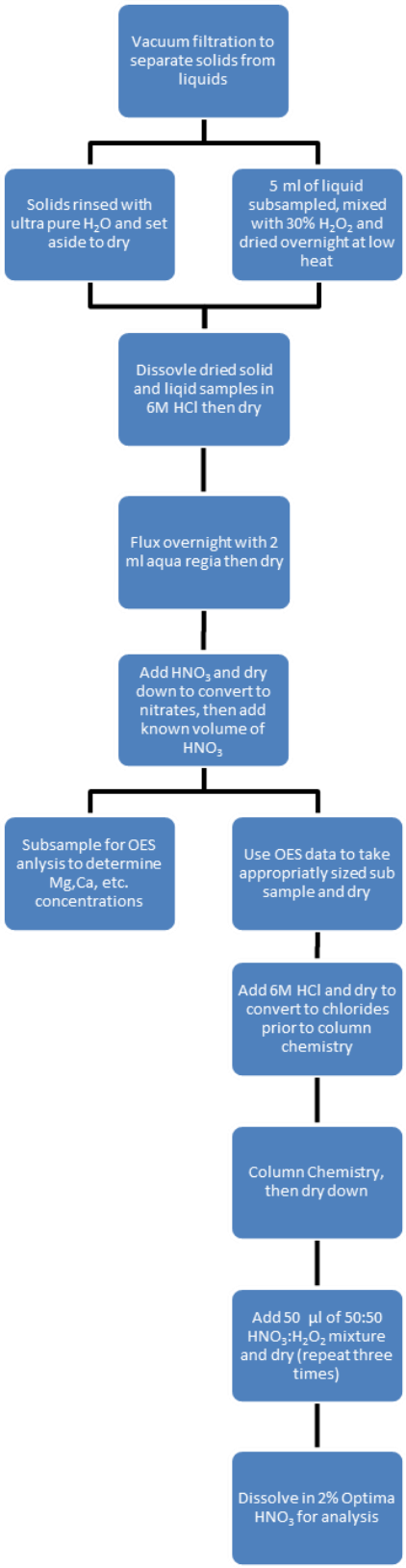

Figure 11. Workflow: Sample preparation for analytical chemistry.

Mass Spectrometry

Magnesium isotope measurements were made at the University of Houston, using a Nu Instruments Plasma II multi -collector inductively-coupled plasma mass spectrometer (MC-ICP-MS). Samples were introduced into the instrument in 2% aqueous HNO_3 using a 20 μl/min teflon nebulizer coupled with a Cetac Aridus II dissolving nebulizer system. Sample solutions were run at a concentration of 2000 ppb. Instrumental mass fractionation effects were corrected via sample-standard bracketing using the NBS980 standard. External precision was calculated using HPS 909104. All data are reported using the standard delta notation (eq. 1) with respect to NBS980.

Chapter 3 - RESULTS

Precipitation During Aerobic Experiments

Precipitation occurred in all aerobic experiments where sterilized cotton plugs allowed exchange with the atmosphere of the laboratory. Precipitation occurred within hours after the containers where plugged, initially proceeding in a similar manner in both the sterile and inoculated samples. At first, thin crusts were formed at the air-water interface or rings around the edge of the container. After approximately 24 hours the inoculated samples became turbid (fig. 12a) and later developed a thin film of organic material at the air-water interface (fig. 13a, b), as well as accumulating a layer of mucilaginous material at the base of the container (fig. 12a). Further precipitation in the inoculated samples occurred more slowly following the formation of the organic film. Eventually isolated cups consisting of hexagonal crystals with hollow stepped upper surfaces similar to "hopper" crystals formed, creating a sheet of hexagonal cups linked together by organic material at their edges (figs.13c and 14a, b). The size of the cups ranged between runs from approximately 0.5-4 mm, with 2-4 mm being common only in the first run and approximately 0.5-1 mm being the most common in subsequent runs. These cups were present in all the inoculated aerobic experiments. In at least one case mineral growth was observed to have also taken place in the mucilaginous material lining the bottom of the inoculated aerobic experiments. SEM images of samples taken from the mucilaginous material of sample O+B+ (4) show several crystal morphologies are present (fig. 15). These crystals differ in appearance from those formed in the organic film and

Figure 12. Photographs of samples in an incubator. (A) Inoculated samples turned hazy after 24 hours and eventually developed a mucilaginous material at the base (arrows), (B) sterile samples remained translucent throughout the experiment, and (C) early precipitation (first 48 hours) at the air-water (arrow) interface.

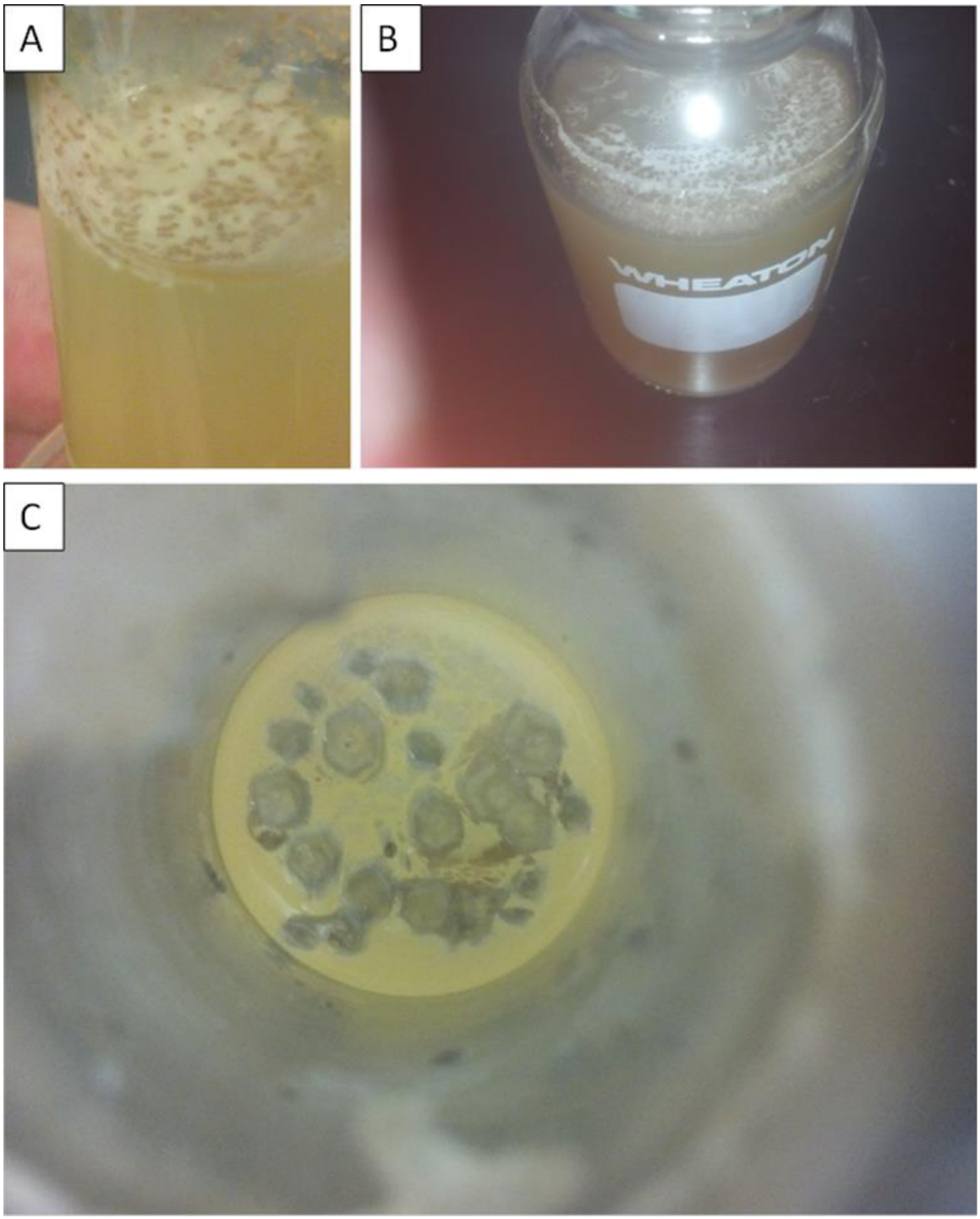

Figure 13. Pictures of precipitates growing in organic film of inoculated samples (A, B) Thin organic film growing along the air-water interface of O+B+ (3) (dia. of container 27 mm) and O+B+ (4) (dia. Of container 55 mm) respectively; precipitates seen growing within this layer grew sometime after the formation of the organic film, (C) well developed hexagonal cups from O+B+ (2) (dia. of container 27 mm), the initial organic film has dissipated. The cups are connected by residual organic material.

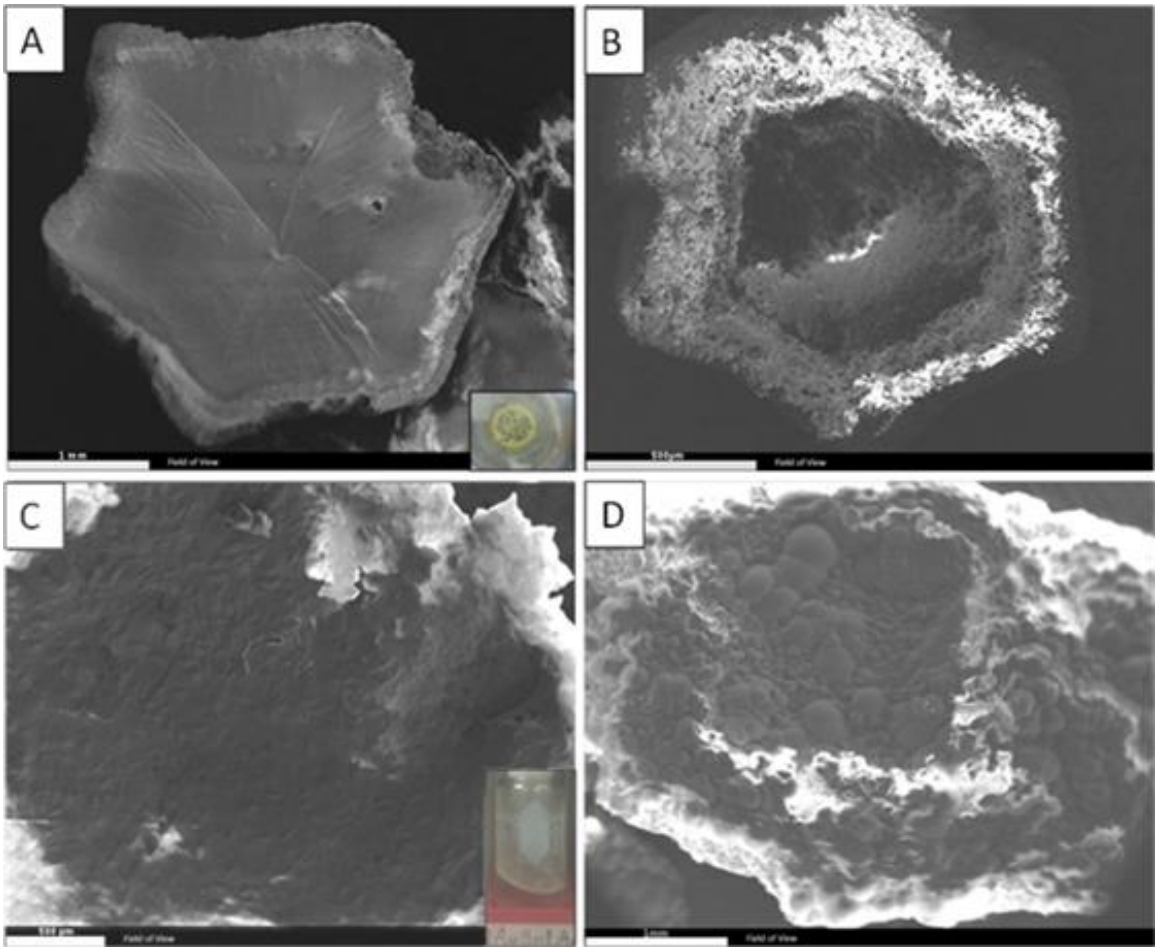

Figure 14. SEM images of precipitates growing in anaerobic inoculated and sterile samples. (A) Top of hexagonal cups found growing in the organic film of O+B+ (2) (white bar is 1 mm), (B) bottom of hexagonal cup, bottom surface is rough in contrast to the smooth upper surface, presumably due to continued crystal growth projecting into the surrounding media (white bar is 500 µm, (C) top of meniscate raft O+B- (3), composed of many smaller interlocking, flat topped crystals terminating against the air-water interface, inset image is a side view of the raft prior to removal for sampling (white bar is 500 µm), and (D) bottom of meniscate raft, hemispheres and various crystal terminations projecting below the surface of the culture media (white bar is 1 mm).

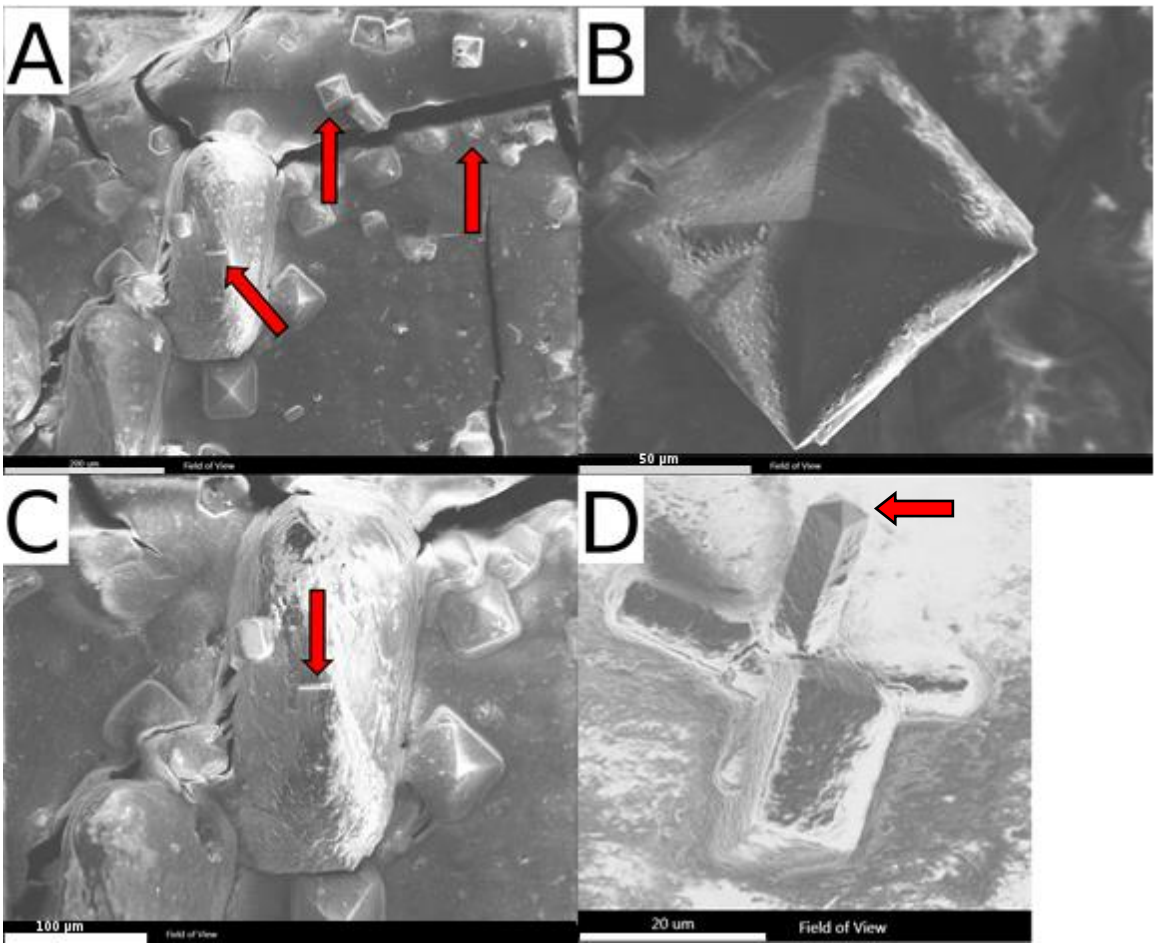

Figure 15. SEM images of precipitates found in mucilaginous material at the base of O+B+ (4). Cracks in the surface are formed as a byproduct of the desiccation of the mucilaginous material. (A) "Pill" and octahedron-shaped crystals and rods (red arrows) (white bar is 200 µm), (B) close-up of octahedron (white bar is 50 µm), (C) close-up of pill-shaped crystal with rod (arrow) (bar is 100 µm), (d) elongated crystal with pyramidal termination (arrow) (white bar is 20 um).

are commonly found in association with rods. The rods measure approximately 25 µm long around bubbles or at the air-water interface (fig. 16b), in some cases producing a meniscate-shaped raft along the air-water interface that under SEM is seen to consist of an amalgamation of intergrown flat-topped crystals (fig. 14c, d). Growth also occurred along the base of the container, with fallen rafts commonly serving as sites for further precipitation.

Precipitation During Anaerobic Experiments

Precipitation was less common in the inoculated and sterile anaerobic samples, only two runs had discernable precipitation. Inoculated anaerobic samples lacking precipitation possessed a pH approximately 5 (table 3) and effervesced violently during pH measurements. Both were likely the result of CO_2 produced by bacteria carrying out fermentation. Similarly precipitation occurred only twice in the sterile anaerobic samples, however, in all cases these samples retained a pH between 7 and 8 (table 3) and where not charged with gas. Precipitation was observed to occur primarily along the sides of some vessels before settling to the base of the container. In some samples, precipitation occurred along the bottom of the containers, forming a thin "frosting" of crystals (fig. 16a, c).

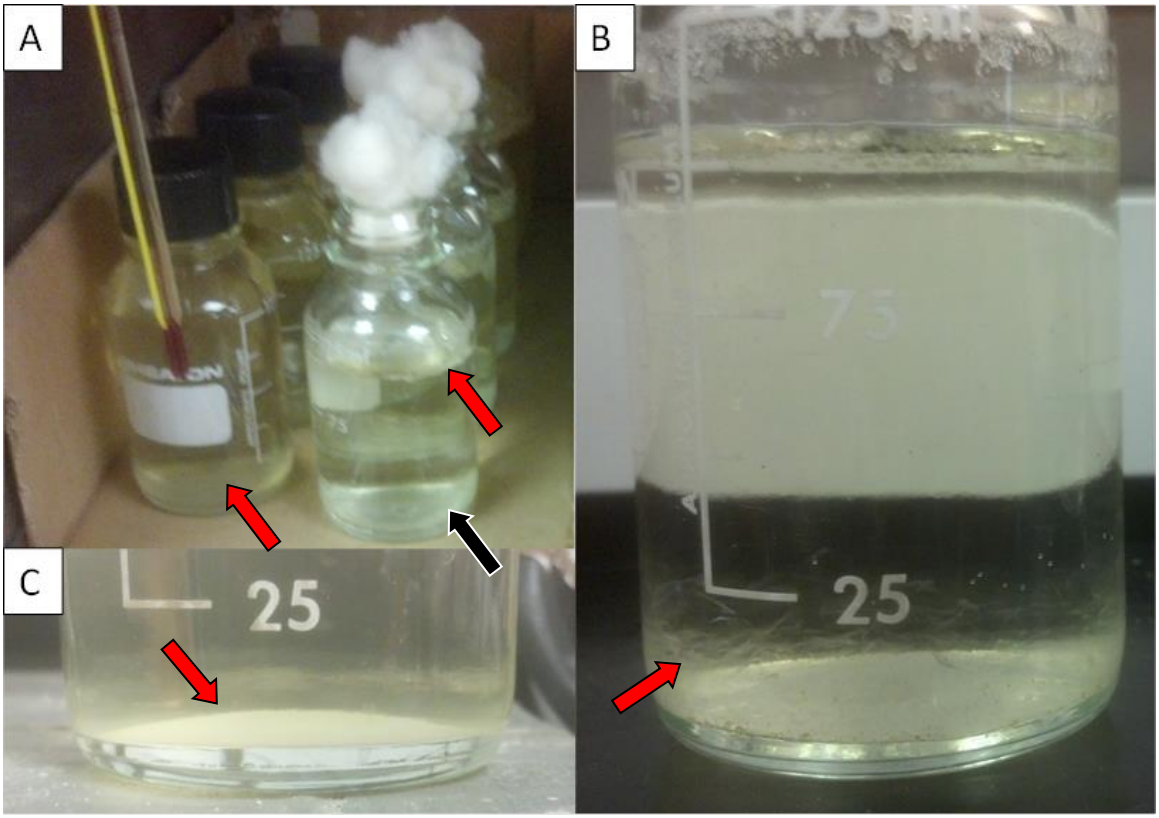

Figure 16. Photographs of precipitates of sterile samples (dia. of all containers 55 mm). (A) Sterile anaerobic with "frosting" of precipitates around bottom (left red arrow) of O-B- (4) and sterile aerobic with rafts at air-water interface (right red arrow), fallen rafts and some precipitation along the container's bottom (black arrow), O+B- (4), (B) close-up of fallen rafts and precipitates along the bottom of O+B- (4) container (red arrow), (C) "frosting" of crystals growing on the base of O-B- (4) container (red arrow).

Mineralogy and Chemical Composition of Precipitates

Mineral phase identification of powdered samples was done with the Match!™ software suite using the supplied COD database (Downs and Hall-Wallace, 2003; Grazulis et al., 2009; Grazulis et al., 2012). Before mineral phase identification, peaks associated with the aluminum sample holder were deleted. The resulting x-ray diffraction patterns can be viewed in the appendix A of XRD data. For samples where sufficient material was obtained for analyses, the identified phases are primarily some variant of magnesian calcite (table 2); any additional precipitates occur in insignificant amounts or likely the result of error due to the small sample sizes available. One notable exception, O+B+ (6), was identified as Kutnohorite ($Ca(Mn^{2+}, Mg, Fe^{2+})(CO_3)_2$), a manganese carbonate mineral and member of the dolomite group (Anthony et al., 2003). Natural samples have been found to contain Mg and Fe substituting for Mn, resulting in a mineral that would produce similar proportions of Mg and Ca as those found in sample O+B+ (6), however, ICP-OES data for sample O+B+ (6) conflicts with the XRD data as insufficient Mn was detected relative to Ca and Mg (Anthony et al., 2003). No studies on magnesium isotope fractionation currently exist for Kutnohorite, however given its similarity to dolomite, it could be expected to show similar biases to those shown in dolomite samples. That is, these samples may be expected to show a smaller fractionation between the culture media and resulting precipitate than observed for calcite (Wang et al., 2003a).

Table 2
Results of XRD analysis

Exp. no.	Mineralogy	Notes
O+B-(2)	Magnesian Calcite	
O+B+(2)	Magnesian Calcite	
O-B-(2)	Calcite	
O-B+(2)	Calcite	
O+B-(3)	Magnesian Calcite	
O+B+(3)	Magnesian Calcite	
O-B-(3)^{ncp}	N/A	Insufficent/No Precipitation
O-B+(3)^{ncp}	N/A	Insufficent/No Precipitation
O+B-(4)	Magnesian Calcite	
O+B+(4)	Magnesian Calcite	
O-B-(4)	N/A	Insufficent Precipitation
O-B+(4)	N/A	Insufficent Precipitation
O+B-(5)	Magnesian Calcite	
O+B+(5)	Magnesian Calcite	
O-B-(5)^{ncp}	N/A	Insufficent/No Precipitation
O-B+(5)^{ncp}	N/A	Insufficent/No Precipitation
O+B-(6)	N/A	Unable to powder sample
O+B+(6)^{ncp}	Kutnohorite	
O-B-(6)^{ncp}	N/A	Insufficent/No Precipitation
O-B+(6)^{ncp}	N/A	Insufficent/No Precipitation

N/A: Not analysed. O+ aerobic O- anaerobic
ncp: no calcite precipitation B+ innoculated B- sterile

Following bulk dissolution, samples were analyzed via inductively coupled plasma optical emission spectrometry (ICP-OES) in order to determine the mole % $MgCO_3$, along with the Mg/Ca ratio of the starting solution, and relative abundance of elements known to cause either isobaric interferences or matrix effects. Samples confirmed to contain calcite ranged from 1.63 to 14.58 mole % Mg calcite (table 3). Other samples labeled ncp were observed to be devoid of calcite precipitation (table 2, 3). Anaerobic samples where no visible precipitation was observed were associated with relatively low concentrations of Mg and Ca measured in samples filtered to collect solids, abnormally high D_{Mg} (Mg partition coefficients), and low pH measurements in inoculated samples. In other cases where XRD analyses were possible, the samples were determined to be devoid of calcite. Sample O+B- (6) did produce sufficient material for XRD analysis, however the resulting sample had a putty like consistency and was unable to be powdered for analysis. Given the fairly high proportion of Mg incorporated and the similarity of its conditions to its inoculated counterpart, it is likely that the resulting mineral was calcite.

The proportion of Mg removed from solution by precipitation varies between experiments from <1% up to 12.5% in samples in which calcite did precipitate. Given the limited reservoir of magnesium available, the isotopic composition of the magnesium incorporated into the solids would have evolved to some extent throughout the process. For experiments where precipitation removed smaller proportions of Mg from the initial solution, the effects would have been minimal. Li et al. (2012) suggest that free drift experiments using <0.5% of the available magnesium would in effect sample an infinite

reservoir. Knowing the extent to which Rayleigh distillation would have differentiated the solution and determining a fractionation factor has been confounded by a large uncertainty in the isotopic data associated with a nonsystematic shift of $\delta^{26/24}$Mg and $\delta^{25/24}$Mg by 0.5‰ and 0.3‰, respectively. The chemical composition before and after precipitation of the solutions used in each run are recorded in table 3. In general, the pH of aerobic experiments increased from the initial solution. The final pH in anaerobic runs ranges both between and within runs. Sterile samples increased, decreased, and maintained starting pH values. Inoculated experiments experienced an increase in pH associated with the formation of precipitates or had a significant drop in pH and no signs of precipitation. The latter is thought to be the result of excessive CO_2 production by anaerobes; the common factor between samples lacking fermentation appears to be lower initial concentrations of magnesium. What variation exists in duration, container volume, initial calcium concentration, and initial pH do not otherwise appear to have effected whether fermentation occurred.

Table 3
Conditions for free drift experiments

Exp. no.	T (°C)	$\Delta^{26/24}$Mg (‰)	Starting pH*	Initial Ca conc. (mMol/L)*	Initial Mg conc. (mMol/L)*	Mg/Ca molar ratio*	Exp. duration (days)	Ending pH	Final Ca conc. (mMol/L)**	Final Mg conc. (mMol/L)**	Mass of precipitate (g)**	%$MgCO_3$**	D_{Mg}**
O+B-(2)	25	-1.01	7.09	44.19	8.93	0.20	77	8.20	34.56	8.71	0.0349	2.24	0.11
O+B+(2)	25	-0.95	7.09	44.19	8.93	0.20	77	8.21	35.21	8.78	0.0324	1.68	0.08
O-B-(2)	25	-1.03	7.09	44.19	8.93	0.20	77	8.25	41.34	8.89	0.0119	1.63	0.08
O-B+(2)	25	-0.35	7.09	44.19	8.93	0.20	77	8.19	37.87	8.78	0.0265	2.32	0.12
O+B-(3)	25	-2.08	7.36	56.05	55.18	0.98	154	8.19	35.37	53.89	0.1045	5.85	0.06
O+B+(3)	25	-1.77	7.36	56.05	55.18	0.98	154	8.64	25.68	53.34	0.1533	5.72	0.06
O-B-(3)^{ncp}	25	0.05	7.36	56.05	55.18	0.98	154	7.44	55.66	55.06	0.0026	22.53	0.30
O-B+(3)^{ncp}	25	-0.34	7.36	56.05	55.18	0.98	154	5.40	55.74	55.03	0.0023	32.53	0.49
O+B-(4)	25	-2.32	7.52	22.69	11.53	0.51	113	8.60	2.54	10.35	0.2222	5.55	0.12
O+B+(4)	25	-2.41	7.52	22.69	11.53	0.51	113	8.68	1.22	10.09	0.2384	6.30	0.13
O-B-(4)	25	-1.5	7.52	22.69	11.53	0.51	113	7.13	22.38	11.51	0.0051	6.72	0.14
O-B+(4)	25	-0.34	7.52	22.69	11.53	0.51	113	7.82	22.62	11.53	0.0011	6.14	0.13
O+B-(5)	25	-2.74	7.34	25.22	34.08	1.35	110	8.20	11.28	31.70	0.1675	14.58	0.13
O+B+(5)	25	-2.25	7.34	25.22	34.08	1.35	110	7.91	6.27	32.85	0.2100	6.10	0.05
O-B-(5)^{ncp}	25	N/A	7.34	25.22	34.08	1.35	110	6.91	20.13	31.71	0.0993	24.05	0.23
O-B+(5)^{ncp}	25	-0.68	7.34	25.22	34.08	1.35	110	5.33	25.19	34.02	0.0012	65.79	1.42
O+B-(6)	25	-1.64	7.29	14.81	83.21	5.62	90	8.28	11.33	81.52	0.0515	32.73	0.09
O+B+(6)^{ncp}	25	-3.39	7.29	14.81	83.21	5.62	90	7.92	9.64	81.55	0.0690	24.23	0.06
O-B-(6)^{ncp}	25	-1.04	7.29	14.81	83.21	5.62	90	6.81	14.80	83.16	0.0007	90.27	1.65
O-B+(6)^{ncp}	25	-1.07	7.29	14.81	83.21	5.62	90	4.39	14.80	83.16	0.0007	86.41	1.13

N/A: Not analysed.
ncp: no calcite precipitation
D_{Mg}: (Mg/Ca) solid/(Mg/Ca) solution
* Measurements taken of initial solution composition
O+ aerobic
O- anaerobic
** Calculated from bulk dissolution of precipitates
B+ innoculated
B- sterile

Magnesium Isotope Fractionation

Delta values for the initial and final solution composition, the precipitates, along with the corresponding Mg sources can be found in table 4. The $\delta^{26/24}$Mg values for the experiments show the expected trend of carbonate phases enriched in lighter isotopes of magnesium relative to the initial solution and an obviously depleted final solution composition in cases where the magnesium removed from solution by precipitation was enough to noticeably shift its composition. In all cases in which calcite precipitation took place $\Delta^{26/24}$Mg was within the ranges reported for marine carbonates ($\Delta^{26}Mg_{calcite\text{-}solution}$ = -1.19 to -4.48‰). In some cases, $\Delta^{26/24}$Mg was below the range found for inorganically synthesized samples ($\Delta^{26}Mg_{calcite\text{-}solution}$ = -3.16 to -1.33 ‰) (Immenhauser et al., 2010; Saulnier et al., 2012; Li et al., 2012; Mavromatis et al., 2013). This deviation from the ranges for laboratory synthesized samples is seen in both organic and inorganic samples and may be explained by some effect on magnesium isotope fractionation that is inherent to the ingredients of the culture media, or in the case of the inoculated samples some effect of microbial activity.

A few overall trends exist in the data for calcite samples. Increasingly negative $\Delta^{26}Mg_{calcite\text{-}solution}$ values are weakly correlated with both increasing amounts of precipitation (R^2=0.74), larger proportions of the available magnesium being incorporated into the solid (R^2=0.52), and being precipitated from solutions with higher Mg/Ca ratios (R^2=0.52) (fig. 17a, b, c). There does not appear to be any clear correlation between D_{Mg} (magnesium partition coefficient) and $\Delta^{26}Mg_{calcite\text{-}solution}$ (R^2=0.02) (fig. 17d).

Table 4
Magnesium isotope composition of solutions and carbonates in synthesis experiments and corresponding isotope fractionation factors

Exp. no.	T (°C)	Mg/Ca	Solution						Carbonates						Fractionation			
			$\delta^{26/24}$Mg	2 SD	$\delta^{25/24}$Mg	2 SD	n	N	$\delta^{26/24}$Mg	2 SD	$\delta^{25/24}$Mg	2 SD	n	N	$\Delta^{26/24}$Mg	2 SD	$\Delta^{25/24}$Mg	2 SD
0.5 $MgCl_2$*			2.18	0.05	1.09	0.05	1	1										
3 $MgCl_2$**			1.67	0.05	0.84	0.05	1	1										
Initial Sol (2)			2.24	0.05	1.14	0.05	6	1										
O+B-(2)	25	0.20	2.42	0.05	1.23	0.05	1	1	1.40	0.05	0.71	0.05	1	1	-1.01	0.07	-0.52	0.08
O+B+(2)	25	0.20	2.48	0.05	1.26	0.05	2	1	1.53	0.05	0.76	0.05	1	1	-0.95	0.07	-0.50	0.08
O-B-(2)	25	0.20	2.28	0.05	1.15	0.05	2	1	1.25	0.05	0.64	0.05	1	1	-1.03	0.07	-0.51	0.08
O-B+(2)	25	0.20	2.24	0.05	1.14	0.05	1	1	1.89	0.05	0.94	0.05	1	1	-0.35	0.07	-0.19	0.08
Initial Sol (3)			1.92	0.11	0.94	0.07	3	1										
O+B-(3)	25	0.98	2.34	0.05	1.17	0.05	1	1	0.25	0.05	0.12	0.05	1	1	-2.08	0.07	-1.05	0.08
O+B+(3)	25	0.98	2.10	0.05	1.04	0.05	1	1	0.34	0.05	0.18	0.05	1	1	-1.77	0.07	-0.87	0.08
O-B-(3)^{ncp}	25	0.98	1.96	0.05	0.97	0.05	1	1	2.01	0.05	1.01	0.05	1	1	0.05	0.07	0.05	0.08
O-B+(3)^{ncp}	25	0.98	2.45	0.05	1.19	0.05	1	1	2.11	0.05	1.07	0.05	1	1	-0.34	0.07	-0.12	0.08
Initial Sol (4)			1.71	0.11	0.85	0.07	3	1										
O+B-(4)	25	0.51	2.07	0.05	1.07	0.05	1	1	-0.25	0.05	-0.16	0.05	1	1	-2.32	0.07	-1.22	0.08
O+B+(4)	25	0.51	2.37	0.11	1.19	0.05	1	1	-0.04	0.11	-0.03	0.05	1	1	-2.41	0.15	-1.23	0.11
O-B-(4)	25	0.51	2.92	0.11	1.48	0.07	1	1	1.42	0.11	0.73	0.07	1	1	-1.50	0.15	-0.75	0.11
O-B+(4)	25	0.51	1.74	0.05	0.87	0.05	1	1	1.40	0.05	0.68	0.05	1	1	-0.34	0.07	-0.19	0.08
Initial Sol (5)			2.73	0.11	1.38	0.07	3	1										
O+B-(5)	25	1.35	2.79	0.11	1.42	0.07	1	1	0.05	0.11	0.00	0.07	1	1	-2.74	0.15	-1.42	0.11
O+B+(5)	25	1.35	2.66	0.11	1.35	0.07	1	1	0.41	0.11	0.20	0.07	1	1	-2.25	0.15	-1.15	0.11
O-B-(5)^{ncp}	25	1.35	2.71	0.11	1.36	0.07	1	1	N/A	N/A	N/A	N/A	N/A	N/A	N/A	N/A	N/A	N/A
O-B+(5)^{ncp}	25	1.35	2.73	0.11	1.38	0.07	1	1	2.05	0.11	1.04	0.07	1	1	-0.68	0.15	-0.34	0.11
Initial Sol (6)			2.21	0.11	1.11	0.07	3	1										
O+B-(6)	25	5.62	2.36	0.11	1.21	0.07	1	1	0.72	0.11	0.34	0.07	2	1	-1.64	0.15	-0.87	0.11
O+B+(6)^{ncp}	25	5.62	2.28	0.11	1.17	0.07	1	1	-1.10	0.11	-0.60	0.07	1	1	-3.39	0.15	-1.76	0.11
O-B-(6)^{ncp}	25	5.62	2.03	0.11	1.02	0.07	12	1	0.99	0.11	0.46	0.07	2	1	-1.04	0.15	-0.56	0.11
O-B+(6)^{ncp}	25	5.62	2.25	0.11	1.12	0.07	1	1	1.18	0.11	0.59	0.07	1	1	-1.07	0.15	-0.53	0.11

N/A: Not analysed.
n: number of analyses.
N: number of replicates.
* Mg Source (2), (3), (4), (5)
** Mg Source (6)
ncp: no calcite precipitation
O+ aerobic
O- anaerobic
B+ innoculated
B- sterile
2 SD

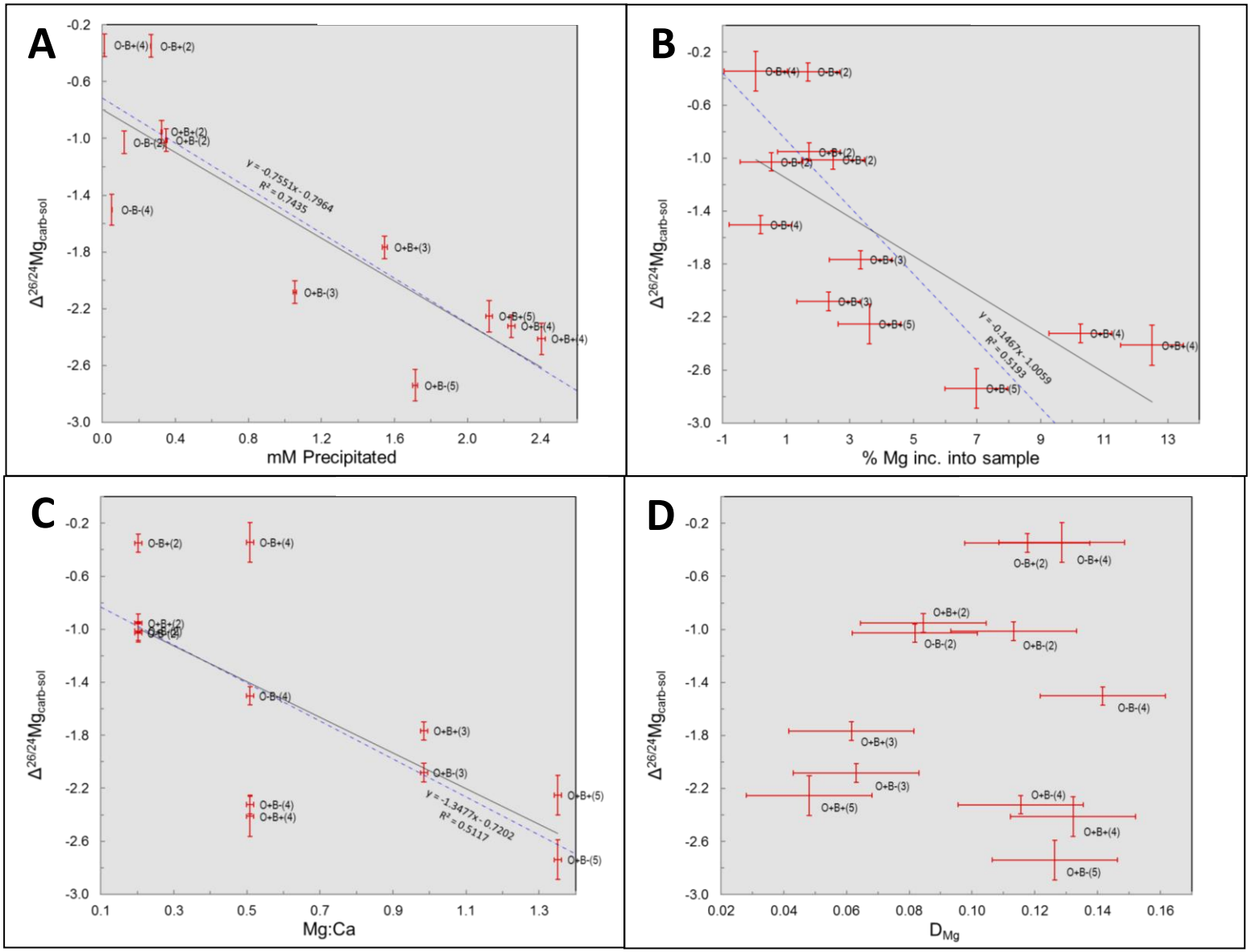

Figure 17. $\Delta^{26}Mg_{calcite\text{-}solution}$ vs : (A) to mM precipitated, (B) % Mg incorporated into the precipitates, (C) Mg:Ca of solution, and (d) D_{Mg} of precipitate; data-point error crosses are 2σ, dashed trend lines are linear regressions using excel and report "goodness" using R^2, solid trend lines use Isoplot's York fit.

Looking closer at runs (2) and (4), the $\Delta^{26}Mg_{calcite\text{-}solution}$ values of the inoculated anaerobic samples for runs (2) and (4) differ greatly from the remaining members of their runs, being much less negative. Additionally, in run (2) the remaining sterile and inoculated variations were nearly identical. Run (4) is similar, however, whereas the $\Delta^{26}Mg_{calcite\text{-}solution}$ of O-B-(4) is more negative than O-B+(4), it is less so than the aerobic samples. Given the similarity of $\delta^{26/24}Mg$ and $\delta^{25/24}Mg$ between the calcite samples of O-B-(4) and O-B+(4) and the significant difference of their solution samples, it is also possible that the water solution sample analyzed for O-B-(4) was contaminated. Substituting the $\delta^{26/24}Mg$ of O-B+(4) yields a $\Delta^{26}Mg_{calcite\text{-}solution}$ nearly identical to O-B+(4). Therefore, in run (2) it would appear that the presence of microorganisms was unique in influencing Mg isotope fractionation in an anaerobic setting, whereas in run (4) the relationship is less clear. Looking further into run (2), the amount of precipitate, proportion of magnesium carbonate, and the amount of Mg removed by precipitation do not correlate with the differences in $\Delta^{26}Mg_{calcite\text{-}solution}$. Run (4) is similar in most regards to run (2), however, if O-B-(4) did in fact have a $\Delta^{26}Mg_{calcite\text{-}solution}$ similar to its inoculated counterpart, it would appear that the amount of precipitation and Mg used does correlate with more negative $\Delta^{26}Mg_{calcite\text{-}solution}$ values. If this is the case, it is odd that increased consumption of Mg during precipitation from a limited reservoir of Mg resulted in calcite further depleted in ^{26}Mg. Given calcite's tendency to be depleted in lighter Mg isotopes relative to the solution from which it precipitates, if Rayleigh fractionation was occurring the inverse would be expected. One possibility is contamination of the samples by the solution, with the smaller anaerobic samples being more easily shifted towards the solution's isotopic composition. This does not seem to be

the case as the solid samples were rinsed repeatedly with ultrapure water during filtration as a preventative measure and the precipitates do not have the elevated proportions of Mg that would be otherwise expected, even in the smaller samples. Unfortunately, in the absence of calcite precipitation in other anaerobic experiments as well as the ambiguity of run (4) it is difficult to definitively answer this question.

Chapter 4 - Discussion

Analytical Considerations

The difficulty of identifying definitive trends within the data and inconsistency between experiments is likely due in part to non-systematic shifts of the measured $\delta^{26/24}$Mg and $\delta^{25/24}$Mg values thought to be associated with incorporation of organic material in the analyzed samples. These contaminants appear to be introduced by the Mg purification process itself, showing up as a discoloration of the dried processed sample prior to additions of concentrated HNO_3 and H_2O_2. Notably, solutions containing approximately 10,000ng Mg sourced from the NBS 980 standard showed a substantial and inconsistent shift towards the negative in measured values of $\delta^{26/24}$Mg and $\delta^{25/24}$Mg (table 1). Previous column calibrations evaluated via quadrupole-ICPMS obtained yields >99%. Additionally, an incomplete yield due to Mg being retained on the column would likely result in a sample with more positive $\delta^{26/24}$Mg and $\delta^{26/24}$Mg values than those measured (table 1), as the resin would preferentially retain the lighter Mg isotopes (Chang et al., 2003; Teng et al., 2007). It is therefore most likely that the cause rests in some residual impurity introduced during the purification process, with some possible contribution from the culture media in experimental samples. In either case, measurements of the initial solution used for each run also differ up by 0.5‰ for $\delta^{26/24}$Mg and 0.3‰ for $\delta^{25/24}$Mg suggesting that the shift seen in the test solutions is also present, and similarly inconsistent. Data generated from an initial attempt to process subsamples of run (2) using the first half of the method of Wombacher et al. (2009) show a

substantial shift between subsamples run initially without additions of a HNO_3 and H_2O_2 mixture and unused portions of the same subsample that were then dried and oxidized (table 5). Oddly enough, the direction and amount of the shift following the oxidation of the residual organics varied in-between samples. These samples were also observed to be discolored only after being passed through the first half of the total procedure, suggesting that at least in some part, organic material is contributed at this step in the overall purification process, possibly a consequence of the concentrated acid used to elute the magnesium degrading the resin. Data from the oxidized second attempt (table 5(2')) differ from a subsample of run (2) processed using the full procedure of Wombacher et al. (2009). This may be in part due to removal of some amount of the organics during the second step, but is also likely associated with the "matrix" eluted in the second step still remaining in the earlier attempts. In spite of the prior removal of Fe and Al, the remaining matrix material would have consisted of enough Na to have exceeded the 0.05 molar ratio of [K+Ca+Na]/[Mg] suggested by Young and Galy et al., (2004).

It is difficult to be sure how effective efforts to remove all the organic material were from sample to sample or if it would even be possible. If organic material was contributed by the experimental samples, it would have to have survived dissolution in 6M HCl (after being heated with concentrated H_2O_2 in the case of the solution samples), being fluxed with aqua regia overnight at 130 °C, and finally being dried multiple times with additions of a concentrated HNO_3 and H_2O_2 mixture following Mg purification. The organics from the column would have at least undergone the last portion of these efforts, and in either case it would appear that fully removing the contaminants would require fairly extreme measures. Either the organics would need to be identified and a suitable

Table 5

Magnesium isotope composition of solutions and carbonates from initial one step Mg purification process of subsamples of run 2 (2), the same subsamples following oxidation to remove organics (2'), and Mg from a subsample of run 2 processed using the method described above

Exp. no.	T (°C)	Mg/Ca	Solution						Carbonates						Fractionation			
			$\delta^{26/24}$Mg	2 SD	$\delta^{25/24}$Mg	2 SD	n	N	$\delta^{26/24}$Mg	2 SD	$\delta^{25/24}$Mg	2 SD	n	N	$\Delta^{26/24}$Mg	2 SD	$\Delta^{25/24}$Mg	2 SD
0.5 $MgCl_2$*			2.18	0.02	1.09	0.01	1	1										
Initial Sol (2)			2.18	0.09	1.08	0.06												
O+B-(2)	25	0.20	2.67	0.09	1.34	0.06	2	1	0.44	0.09	0.15	0.06	2	1	-2.23	0.13	-1.19	0.09
O+B+(2)	25	0.20	2.63	0.09	1.31	0.06	1	1	0.91	0.09	0.36	0.06	1	1	-1.72	0.13	-0.95	0.09
O-B-(2)	25	0.20	2.19	0.09	1.07	0.06	1	1	0.23	0.09	0.01	0.06	1	1	-1.95	0.13	-1.06	0.09
O-B+(2)	25	0.20	2.29	0.09	1.12	0.06	1	1	1.09	0.09	0.48	0.06	1	1	-1.20	0.13	-0.64	0.09
Initial Sol (2)'			2.49	0.07	1.26	0.03												
O+B-(2)'	25	0.20	2.63	0.07	1.31	0.03	2	1	1.33	0.07	0.64	0.03	1	1	-1.30	0.10	-0.67	0.05
O+B+(2)'	25	0.20	2.50	0.07	1.22	0.03	2	1	0.59	0.07	0.26	0.03	1	1	-1.91	0.10	-0.97	0.05
O-B-(2)'	25	0.20	2.42	0.07	1.23	0.03	2	1	1.21	0.07	0.63	0.03	1	1	-1.20	0.10	-0.61	0.05
O-B+(2)'	25	0.20	2.68	0.07	1.34	0.03	1	1	2.02	0.07	1.05	0.03	1	1	-0.66	0.10	-0.29	0.05
Initial Sol (2)"			2.24	0.05	1.14	0.05	6	1										
O+B-(2)"	25	0.20	2.42	0.05	1.23	0.05	1	1	1.40	0.05	0.71	0.05	1	1	-1.01	0.07	-0.52	0.08
O+B+(2)"	25	0.20	2.48	0.05	1.26	0.05	2	1	1.53	0.05	0.76	0.05	1	1	-0.95	0.07	-0.50	0.08
O-B-(2)"	25	0.20	2.28	0.05	1.15	0.05	2	1	1.25	0.05	0.64	0.05	1	1	-1.03	0.07	-0.51	0.08
O-B+(2)"	25	0.20	2.24	0.05	1.14	0.05	1	1	1.89	0.05	0.94	0.05	1	1	-0.35	0.07	-0.19	0.08

N/A: Not analysed. * Mg Source (2), (3), (4), (5) 2 SD: two standard deviations

n: number of analyses. O+ aerobic O- anaerobic

N: number of replicates. B+ innoculated B- sterile

method for separation prepared or a more powerful oxidizing agent would need to be used. The first option would be cost and time prohibitive, and the second (e.g., $HClO_4$) dangerous. Additionally, alternative procedures using $HClO_4$ to eliminate organic materials have been shown to cause a shift in measured $\delta^{26/24}Mg$ and $\delta^{25/24}Mg$ values (Chang et al., 2003). It would likely be more productive to instead investigate the use of other methods of Mg separation as well as determining if there is a need to improve the procedures for removing organics from the culture media or if using an alternative media would yield better results.

Microbial Influence on Crystal Morphology, Mineralogy, and Chemistry

Given the dissimilarity between the crystal morphologies of the inoculated and sterile aerobic samples it is clear that the microbial activity expresses some control on crystal morphology. Precipitates that formed at the air-water interface in sterile experiments (figs. 11 a, b, c and 12 a, b, c, d) largely consisted of amalgamations of flat-topped calcite rafts wherein growth occurred along the bottom of the rafts. The initial manner of precipitation was similar in both the inoculated and sterile samples. However, the organic film that soon formed in the inoculated samples both slowed the rate at which precipitation occurred, and also produced hexagonal "cups" with stepped euhedral faces in the inside of the "cup". Assuming CO_3 was the limiting reactant, the slower rate at which precipitates formed in the inoculated samples is likely due to the organic film slowing the rate of diffusion of gaseous CO_2 from the surrounding atmosphere, thus retarding mineral growth. The manner of precipitation occurring here appears to be

similar to that of a "cave cup" (Wells, 1971; Merino et al., 2014). The cup shape of these speleothems forms as the water level of a pool rises and additional material is accreted along the edges of the cup growing up and away from the center, further isolating the central area from the surrounding solution. Examples found in the literature are most commonly associated with some initial center of precipitation from which growth continues until the surface is reached (e.g., a fallen stalactite) or form as projections from the edge of the pool (Wells, 1971; Merino et al., 2014). In the inoculated experiments it would appear that the initial center of growth was suspended in the scum. Formation of a cup occurred as the crystal gradually sank in response to new material accreting onto its edges and bottom, creating a hollow upper surface. Thus growth occurred in a manner similar to a stationary cave cup, but with the suspended crystal moving relative to the water's surface. Wells (1971) posits a similar origin for "island growth" in which dust is seen suspended at the surface of a pool and acts as initial nuclei for crystal growth rather than originating from the base or edge of the pool. The "pill"-shaped crystals may have had an origin similar to the "rods" found by Buczynski and Chafetz (1991), possibly entombing colonies of microorganisms. If this was the case the original "rod" shape has long since been over grown as the "pills" are approximately 50 times as long as the examples found by Buczynski and Chafetz (1991) and have some rough anhedral to subhedral crystal faces. Unfortunately, it is difficult to discern the form of the crystals. The octahedrons along with the elongated crystal with the pyramidal termination possess well-developed euhedral faces, but do not appear to be calcite or any other carbonate mineral. No mineral appears in the XRD data that shares the crystal system of the crystals

nor would they have been able to pass through the 0.22 μm membrane used to sterilize the culture media. It may be that these crystals precipitated as a result of the process to desiccate the sample of mucilaginous bottom layer and thus are absent from samples used for XRD analysis. The origin of these crystals and to what degree they are microbial influenced is unclear.

The minerology of the precipitates for runs (2), (3), (4), and (5) is consistently magnesian calcite and are not significantly influenced by microbial activity; the results of run (6) are less clear as there is no XRD data to determine the minerology of O+B- (6), thus it is uncertain if it differs from that of its inoculated counterpart. The only other evidence of microbial influence on "minerology" are the low pH values for the inoculated anaerobic samples lacking precipitation. Their sterile counterparts show that a lack of precipitation may be associated with a solution with insufficient supersaturation to overcome magnesium poisoning associated with elevated concentrations of Mg. Additionally, the proportion of $MgCO_3$ incorporated in an inoculated sample did not systematically increase or decrease relative to its sterile counterpart.

Potential Influences of Microbes on Mg Isotope Fractionation

Whereas inoculated aerobic samples produce crystal morphologies different than their sterile counterparts, it appears that Mg isotope fractionation is controlled or more significantly influenced by the physiochemical conditions and more rapid precipitation. Conversely, the few anaerobic samples present suggest that in anaerobic environments, or simply environments where mineral growth is slowed by the limited availability of CO_3,

microorganisms may exert a control on isotope fractionation that otherwise may be overprinted during more rapid precipitation. Given the inoculated anaerobic samples' tendency to be relatively enriched in heavier isotopes, it is possible that calcite grown in the mucilaginous regions associated with microbial activity would have sampled a microenvironment depleted of lighter Mg. This may be the result of the preferential uptake of lighter Mg by microorganisms or the result of EPS preferentially binding lighter Mg. The latter would be similar to the retention of isotopically light Mg by resin during Mg separation (Chang et al., 2003; Teng et al., 2007). Similarly, isotopically light biogenic HMC is also suggested to be the result of microenvironments created by organisms that use biomolecules to create a locally elevated Mg/Ca ratio. These biomolecules are suggested to also preferentially bind lighter Mg resulting in a similar effect (Saenger and Wang, 2014). Additionally, it may also be possible that the mineral growth seen in the lower mucilaginous region of run (4)'s aerobic samples may have experienced a similar environment, however, this material was not collected separately for analysis.

Alternatively, it has been demonstrated that the precipitation of calcium carbonate within microbial mats is initiated with the formation of amorphous calcium carbonate (ACC) within the EPS (Hammes et al., 2003; Obst et al., 2009). Additionally, the formation of globules consisting of ACC and EPS in the EPS adjacent to sulfate reducing bacteria has also been observed (Aloisi et al., 2007). These amorphous materials are thought to acts as a template for mineral precipitation (Hammes et al., 2003; Aloisi et al., 2007; Dupraz et al., 2008; Obst et al., 2009). No data currently exists for effects of ACC

precipitation on Mg isotope fractionation, however, it is known to fractionate Ca isotopes more weakly (Gagnon et al., 2010). Recent work by Giuffre (2015) suggests that the isotopic composition of an ACC precursor may have little effect on the isotopic composition of the crystalline calcite it transforms into. However, whether this would be the case in the presence of EPS and other organic molecule is unknown. Ultimately the effect that the initiation of calcite growth by ACC produced within the EPS has on the Mg isotope fractionation of calcite grown within the EPS matrix of a microbial mat is unknown.

Physiochemical Conditions Versus Microbial Activity

As previously stated, aerobic experiments appear to be governed by the physicochemical conditions of the experiment, with precipitates growing increasingly depleted in ^{26}Mg with increases in the amount of precipitation, proportional to the available magnesium being incorporated into the solid, and Mg/Ca of the associated solutions with no apparent intervention by microbial activity. Higher Mg/Ca ratios have been shown to slow step velocities until a critical ratio of approximately 1.7 mol/mol has been reached beyond which step velocities are relatively constant (Saenger and Wang, 2014). With the exception of run (6), which failed to produce calcite, all the prior runs were conducted within a range between 0.2 to 1.35 mol/mol Mg/Ca. It may be that the progressive increases in Mg/Ca resulted in progressively slower step velocities thus allowing for an increasing proportion of mineralogical control over the isotopic composition of the resulting precipitates. Therefore calcite's tendency to be depleted in

^{26}Mg relative to the reservoir would be increasing expressed. An explanation of the association with the amount precipitated and proportion of Mg used by the precipitate is more problematic. Given the different volumes between experiments and variation in the concentration of both Mg and Ca, it may be purely coincidental that the amount of precipitate produced appears to correlate with anything. Alternatively, samples with larger amounts of precipitate also tend to have higher proportions of Mg incorporated in most cases. Samples using larger proportions of their respective reservoirs of Mg, however, would be expected to result in isotopic compositions progressively closer to the initial reservoir composition as the reservoir's isotopic compositions evolves.

Overall it appears that microbial activity does have the ability to influence Mg isotope fractionation in calcite through some means, but these also appear to be restricted to either anaerobic environments or microenvironments associated with microbial activity within a matrix of EPS.

Chapter 5 - Conclusions

Free drifts experiments were conducted in order to access whether microbial activity would influence the fractionation of Mg isotopes during calcite precipitation. Evidence of microbial influence presented itself through variations in the crystal morphology of the resulting precipitates as well as the acidification of anaerobic samples associated with the generation of CO_2 gas. This may have been the result of fermentation triggered by elevated Mg concentrations. In experiments using lower concentrations of Mg, precipitates formed in inoculated anaerobic environments resulted in heavier isotopic compositions than sterile anaerobic, as well as sterile and inoculated aerobic samples from the same run. It may be that this is associated with precipitates formed within a microenvironment depleted of lighter Mg isotopes as a result of microbial activity. Similar results within runs of inoculated and sterile aerobic experiments indicate any influence present from microbial activity is largely overridden by physiochemical conditions. Overall trends in the data suggest that elevations in the Mg/Ca ratio of the solution from which precipitation originates and the proportion of Mg used by the precipitate result in increasingly negative $\Delta^{26}Mg_{calcite\text{-}solution}$ values. The former is thought to be related to a steady reduction of calcite step velocities subsequently allowing for an increase in mineralogical control over fractionation, as calcite favors lighter isotopes of Mg. Observations made of isotope data within this study are difficult to present as definitive due in part to nonsystematic shifts in measurements of isotopic composition. These shifts are seen in test solutions created with NBS 980 (table 1), differences in the

starting isotopic composition of runs with identical Mg sources, and differences between the initial isotopic composition of a run and those of its Mg source. This has been found to be the result of unresolvable organic material originating from the purification process and possibly the culture media used during experiments.

Future work

Future work would at a minimum require sorting out the organics originating during the purification process, or more prudently, using a different Mg separation procedure, as well as determining whether the culture media is a source of the detrimental organic materials. If the organics in the media cannot be resolved, further experimentation may require the use of a different culture media. The quality of the data may also be improved by using a mineral standard similar to the carbonates produced to reduce differences between standard and sample matrices as well as running additional isotope systems (e.g., Ca or Sr) and analyzing their behaviors. Further improvements could be made to the experimental process by several means. Utilizing a flow through reactor to create an "infinite reservoir" of Mg, and taking steps to prevent evaporation, would prevent significant differences of the chemical and isotopic composition of the bulk solution sampled by the precipitates. Ideally this should be done in such a way to allow microorganisms to locally influence physiochemical conditions and isotopic composition. Additionally, an improved means of setting the initial saturation state would be desirable. This could be done by purging the initial solution of CO_2 and then supplying

CO_2 by bubbling or diffusion through a membrane similar to the method of Immenhauser et al. (2010).

Appendix A

This appendix contains XRD patterns used in mineral phase analysis of samples which were processed using the Match! software suite using the supplied COD database (Downs and Hall-Wallace, 2003; Grazulis et al., 2009; Grazulis et al., 2012). Each image consists of the pattern generated by the aluminum sample holder displayed above the experimental and calculated patterns for the sample. The grey regions correspond to portions of each pattern that were omitted in order to subtract the sample holder from the analyzed sample. The legends in the images are color coded to their respective counter parts (e.g., the text for experimental pattern and the pattern itself are blue).

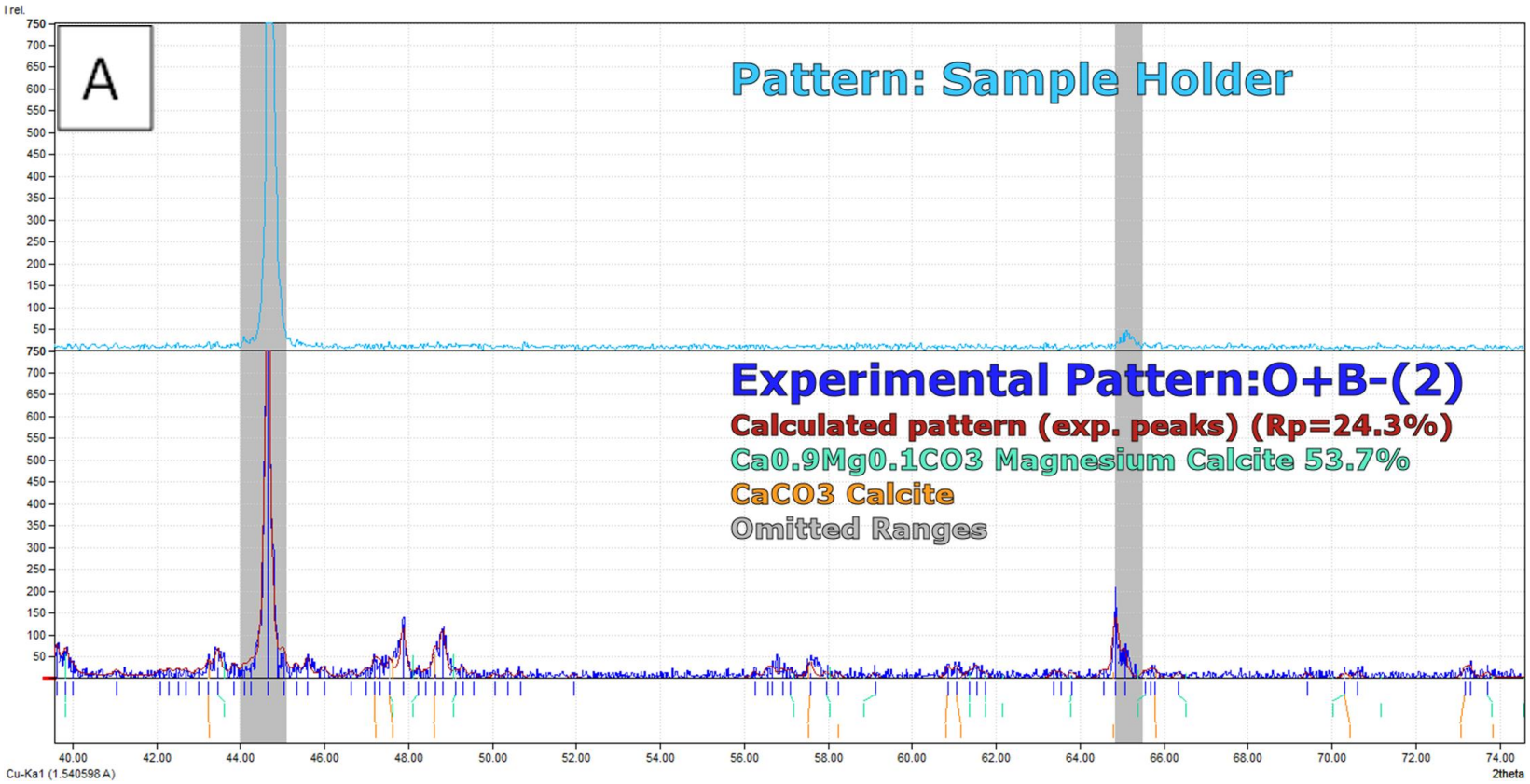
I rel.
A
Pattern: Sample Holder
Experimental Pattern:O+B-(2)
Calculated pattern (exp. peaks) (Rp=24.3%)
Ca0.9Mg0.1CO3 Magnesium Calcite 53.7%
CaCO3 Calcite
Omitted Ranges
Cu-Ka1 (1.540598 A)
2theta

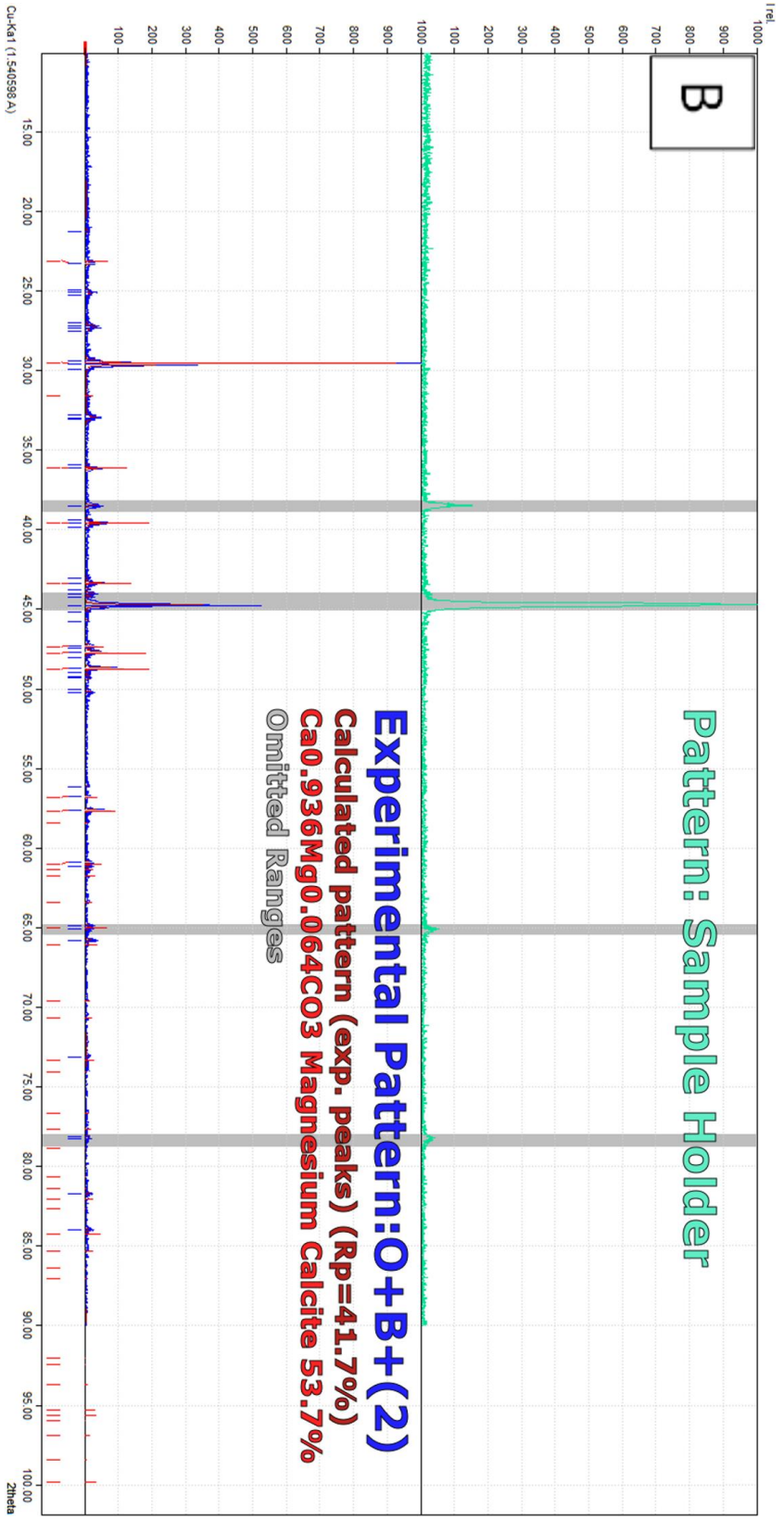
B
Pattern: Sample Holder
Experimental Pattern:O+B+(2)
Calculated pattern (exp. peaks) (Rp=41.7%)
Ca0.936Mg0.064CO3 Magnesium Calcite 53.7%
Omitted Ranges
I rel.
Cu-Ka1 (1.540598 A)
2theta

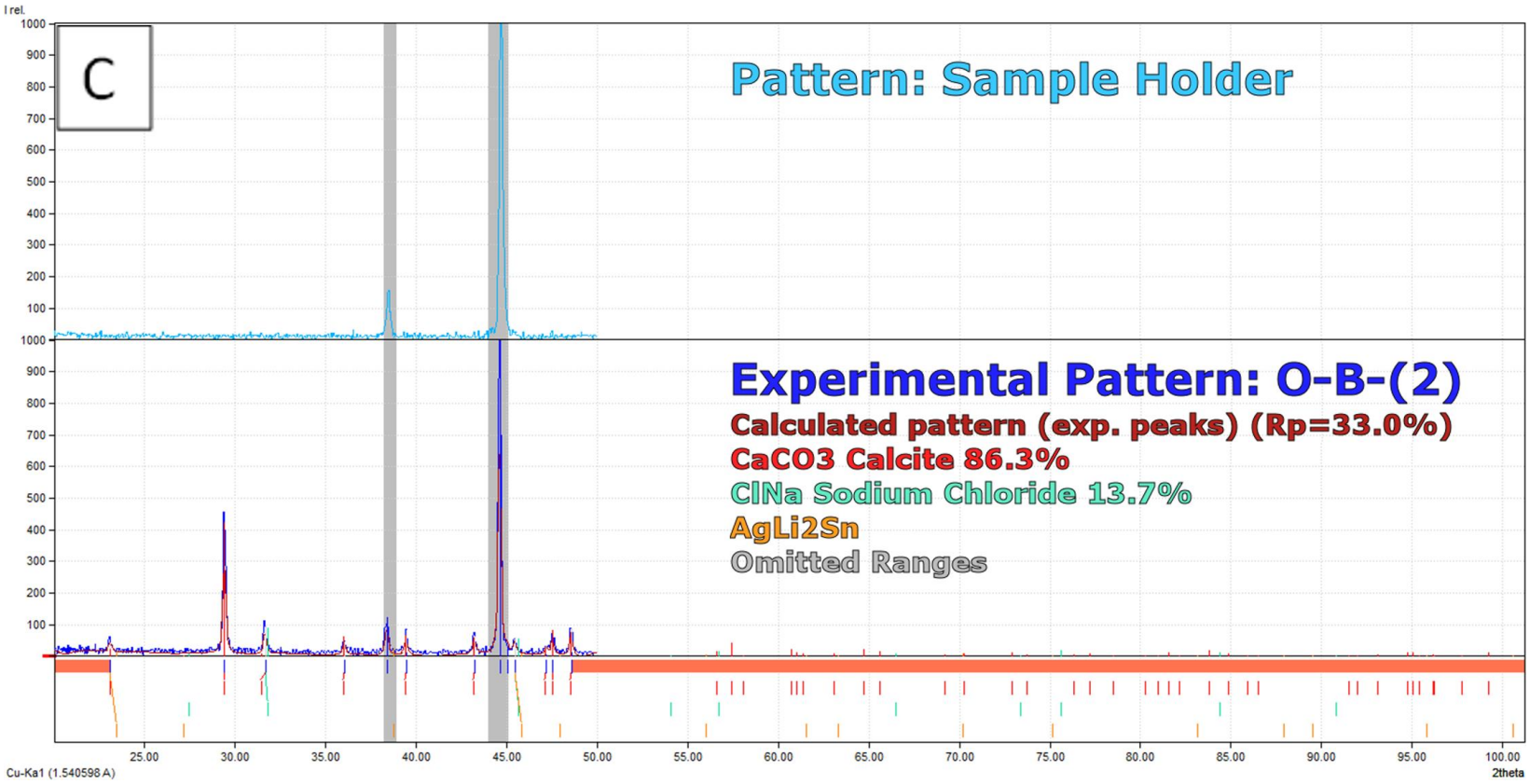
C
Pattern: Sample Holder
Experimental Pattern: O-B-(2)
Calculated pattern (exp. peaks) (Rp=33.0%)
CaCO3 Calcite 86.3%
ClNa Sodium Chloride 13.7%
AgLi2Sn
Omitted Ranges
I rel.
Cu-Ka1 (1.540598 A)
2theta

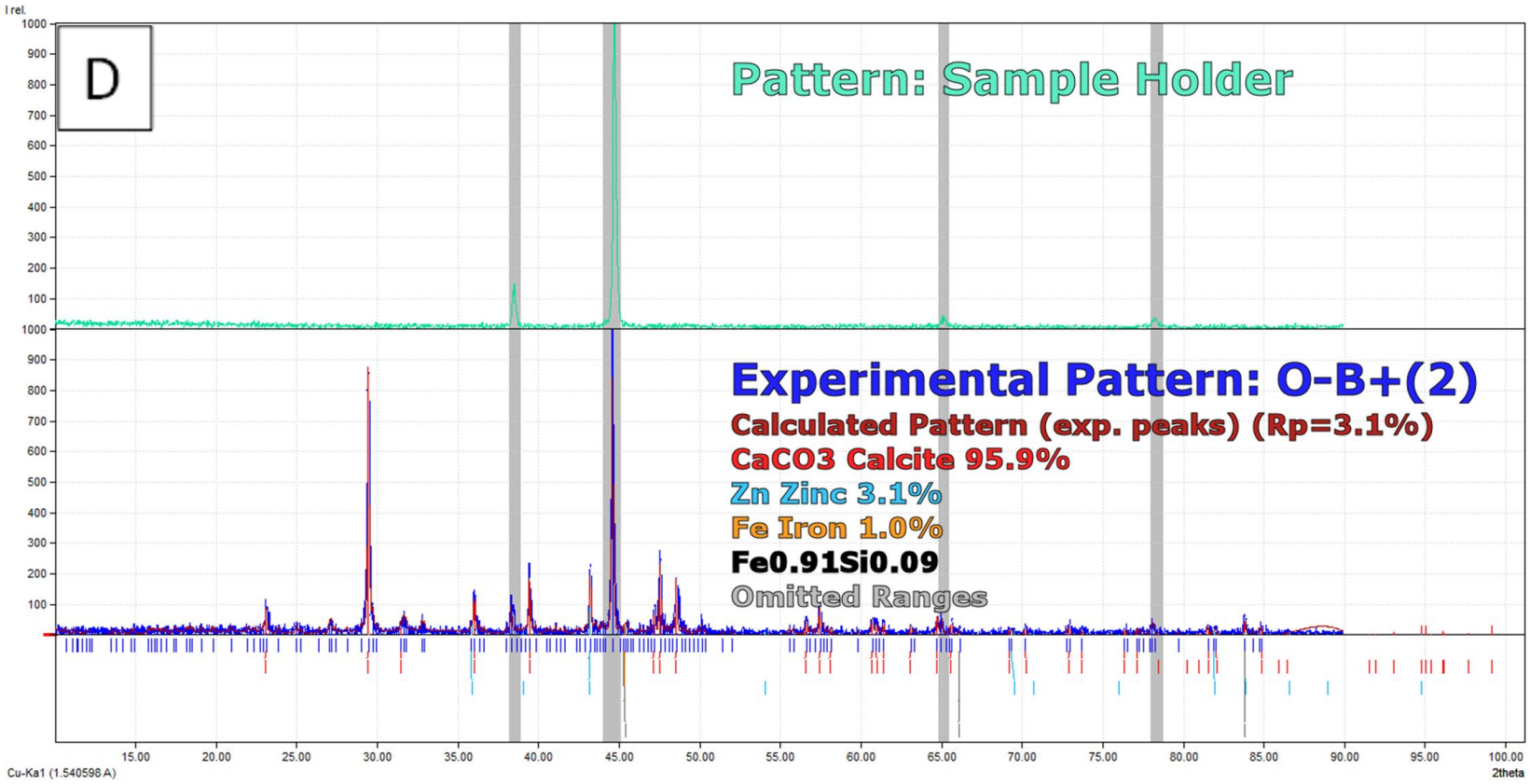
I rel.
D
Pattern: Sample Holder
Experimental Pattern: O-B+(2)
Calculated Pattern (exp. peaks) (Rp=3.1%)
CaCO3 Calcite 95.9%
Zn Zinc 3.1%
Fe Iron 1.0%
Fe0.91Si0.09
Omitted Ranges
Cu-Ka1 (1.540598 A)
2theta

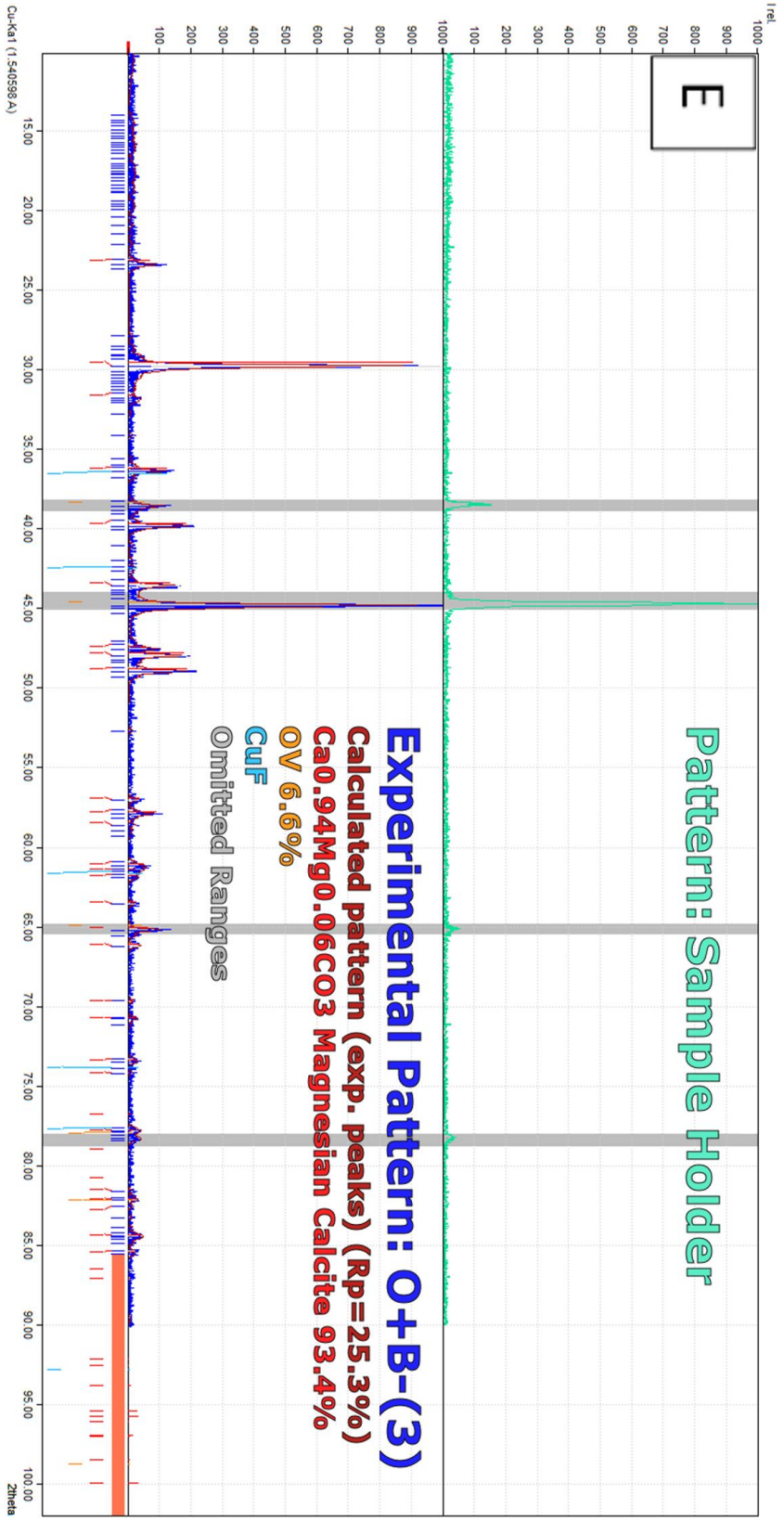
E
Pattern: Sample Holder
Experimental Pattern: O+B-(3)
Calculated pattern (exp. peaks) (Rp=25.3%)
Ca0.94Mg0.06CO3 Magnesian Calcite 93.4%
OV 6.6%
CuF
Omitted Ranges
I rel.
Cu-Ka1 (1.540598 A)
2theta

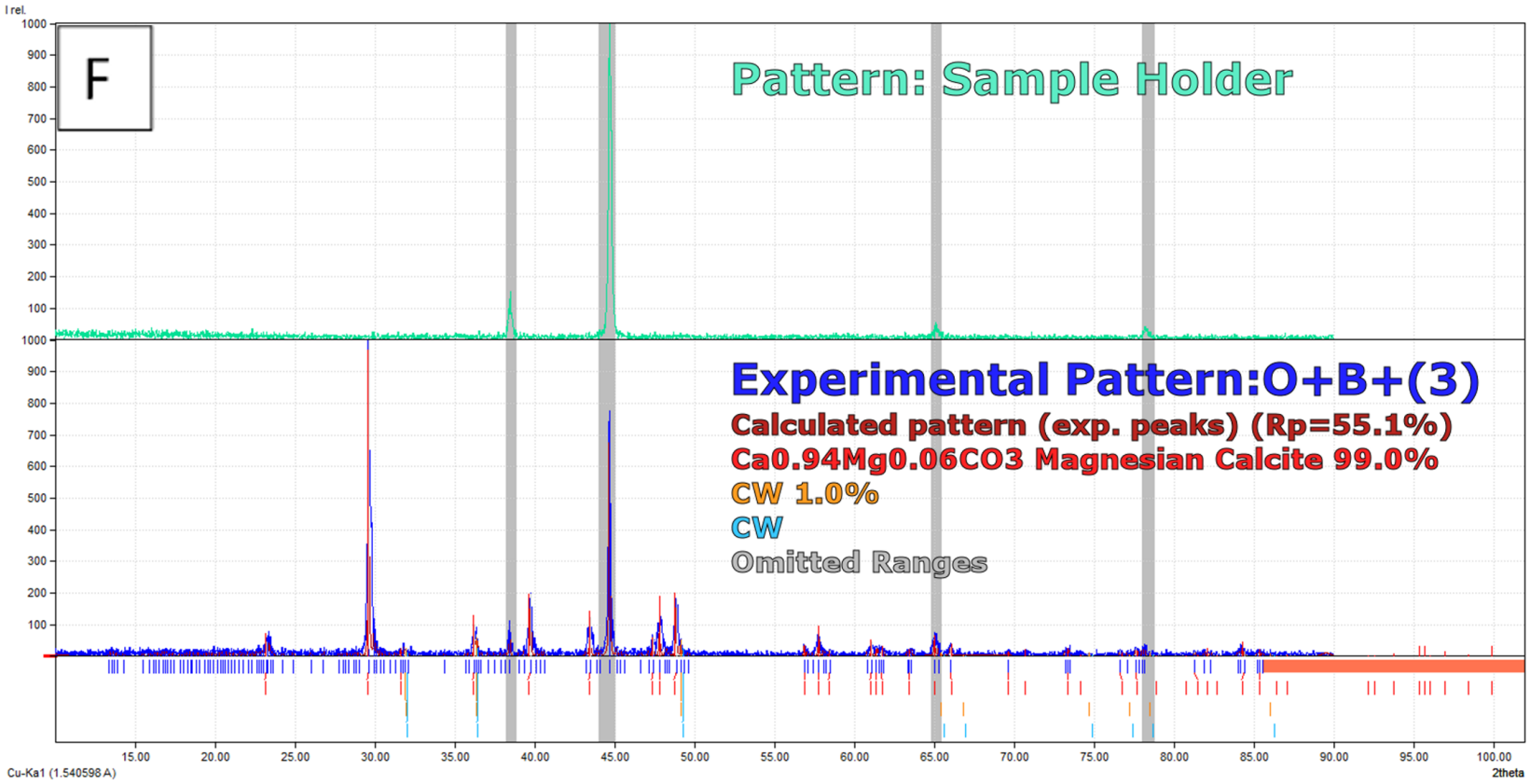
I rel.
F
Pattern: Sample Holder
Experimental Pattern:O+B+(3)
Calculated pattern (exp. peaks) (Rp=55.1%)
Ca0.94Mg0.06CO3 Magnesian Calcite 99.0%
CW 1.0%
CW
Omitted Ranges
Cu-Ka1 (1.540598 A)
2theta

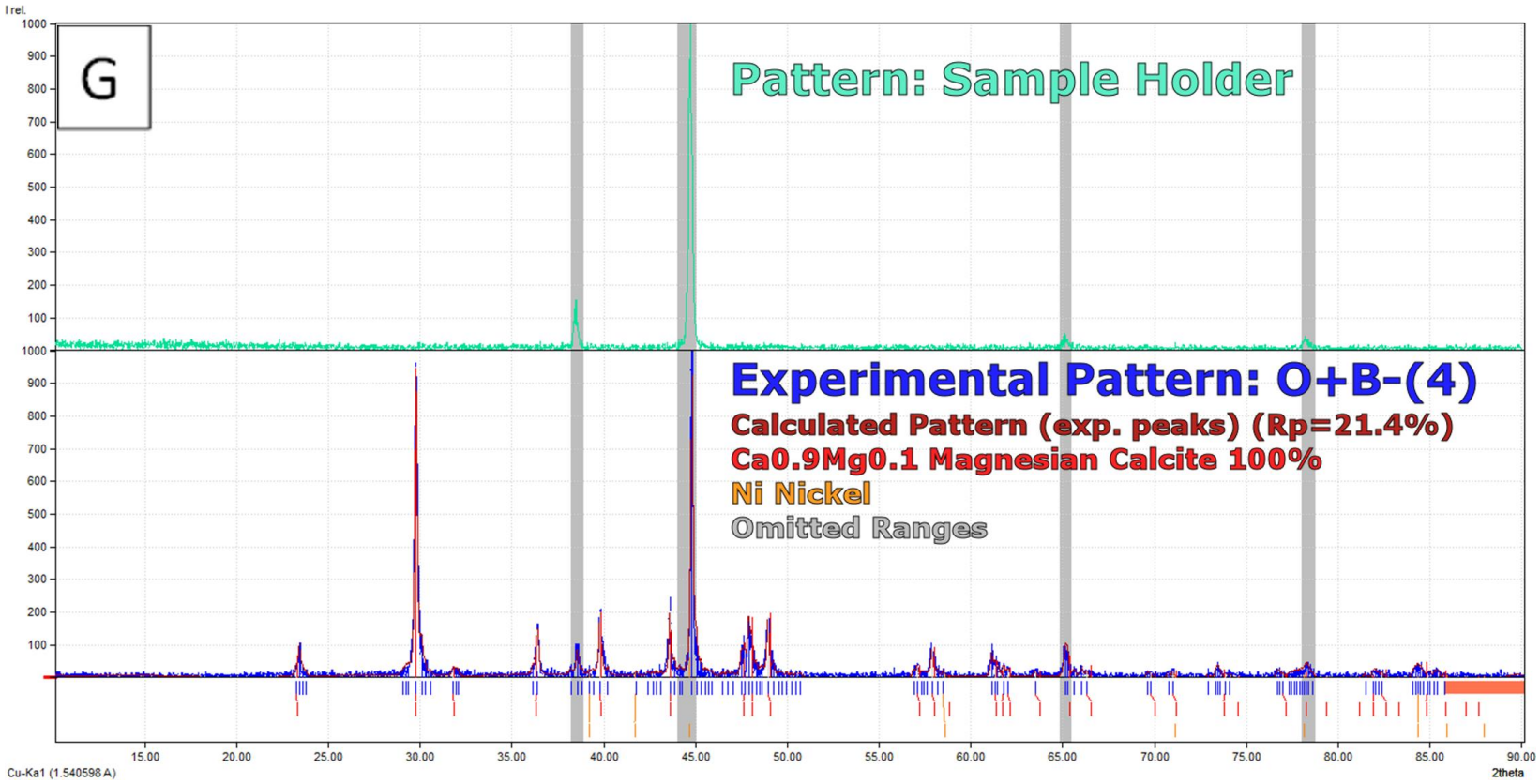
I rel.
G
Pattern: Sample Holder
Experimental Pattern: O+B-(4)
Calculated Pattern (exp. peaks) (Rp=21.4%)
Ca0.9Mg0.1 Magnesian Calcite 100%
Ni Nickel
Omitted Ranges
Cu-Ka1 (1.540598 A)
2theta

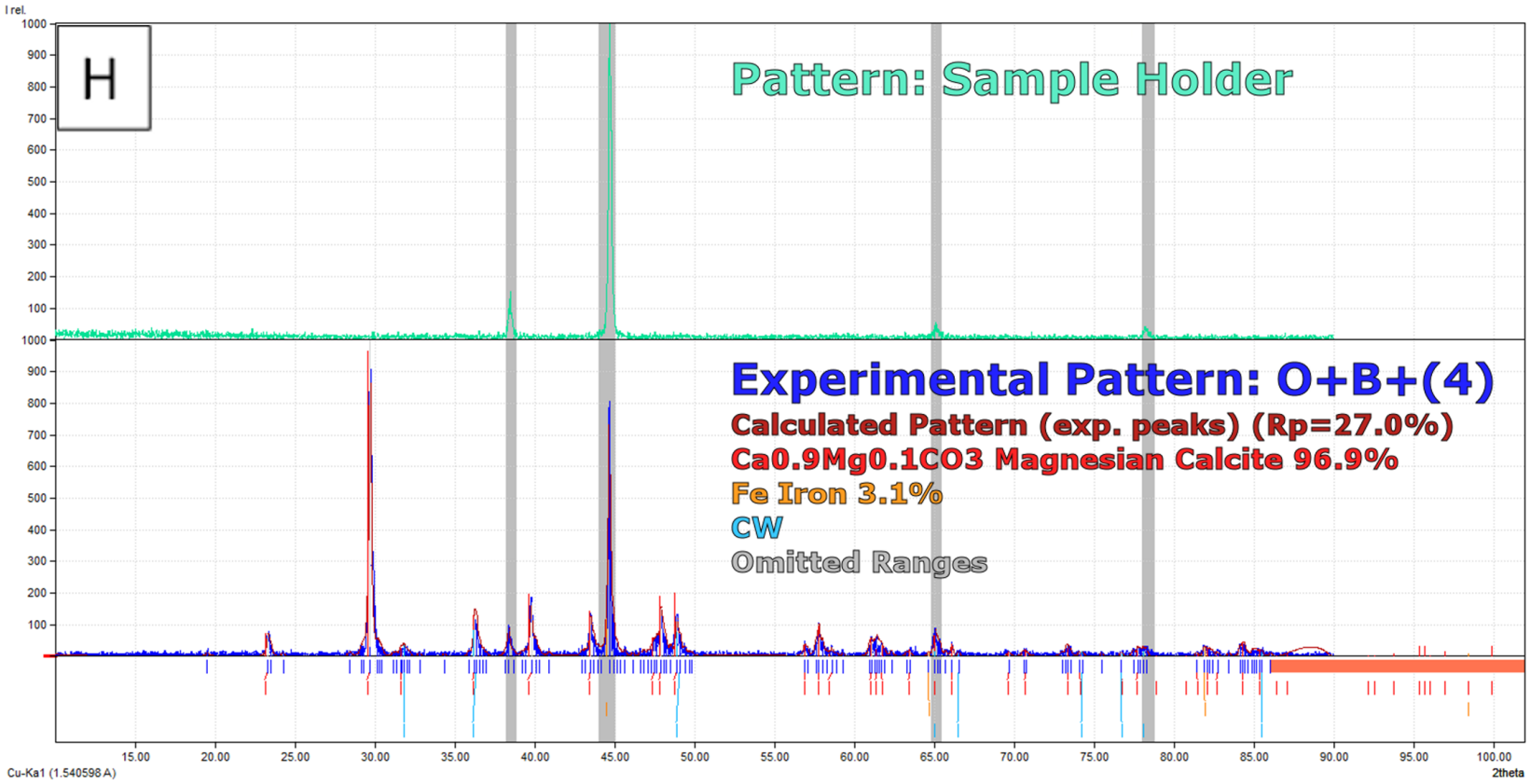
I rel.
H
Pattern: Sample Holder
Experimental Pattern: O+B+(4)
Calculated Pattern (exp. peaks) (Rp=27.0%)
Ca0.9Mg0.1CO3 Magnesian Calcite 96.9%
Fe Iron 3.1%
CW
Omitted Ranges
Cu-Ka1 (1.540598 A)
2theta

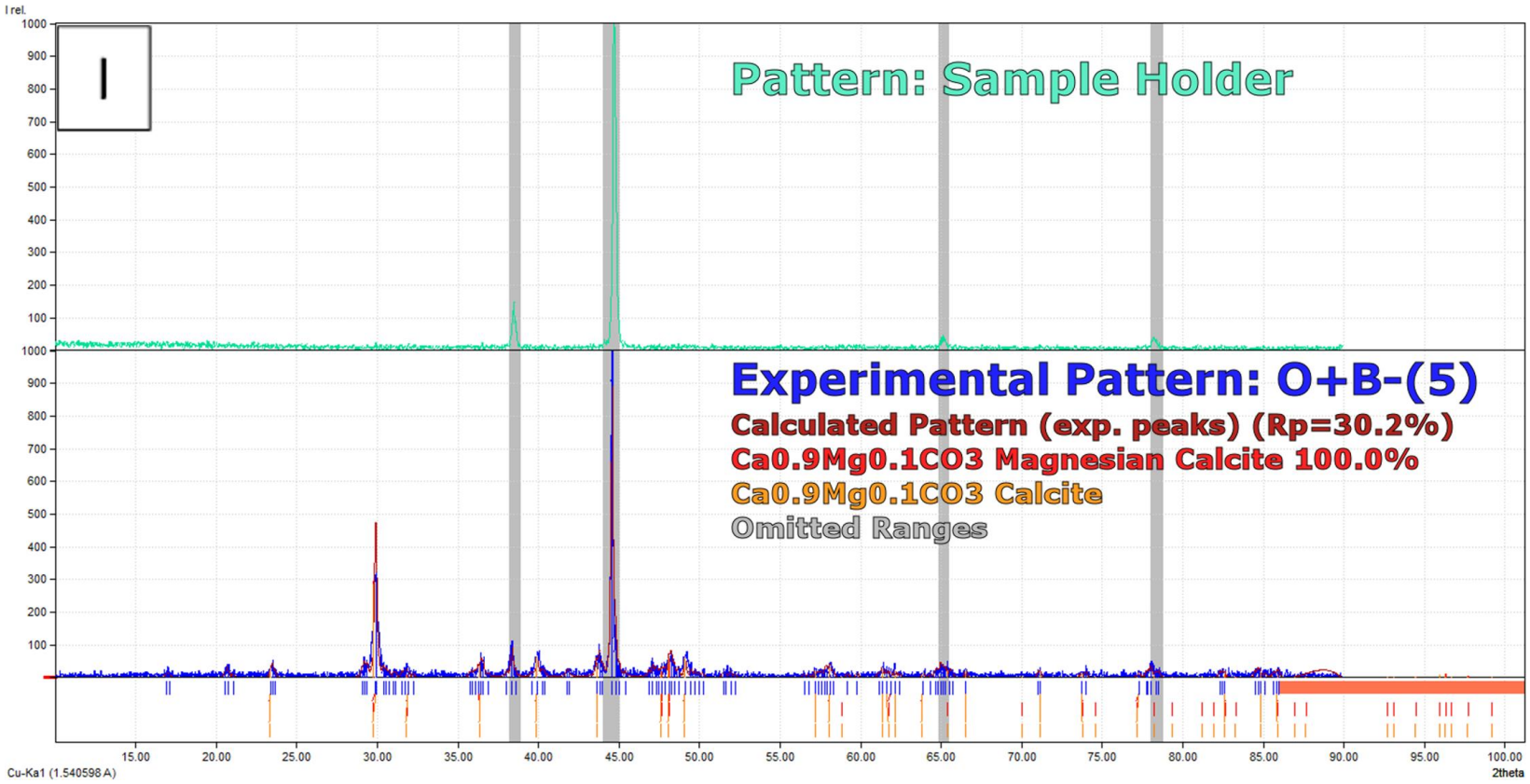
I rel.
Pattern: Sample Holder
Experimental Pattern: O+B-(5)
Calculated Pattern (exp. peaks) (Rp=30.2%)
Ca0.9Mg0.1CO3 Magnesian Calcite 100.0%
Ca0.9Mg0.1CO3 Calcite
Omitted Ranges
Cu-Ka1 (1.540598 A)
2theta

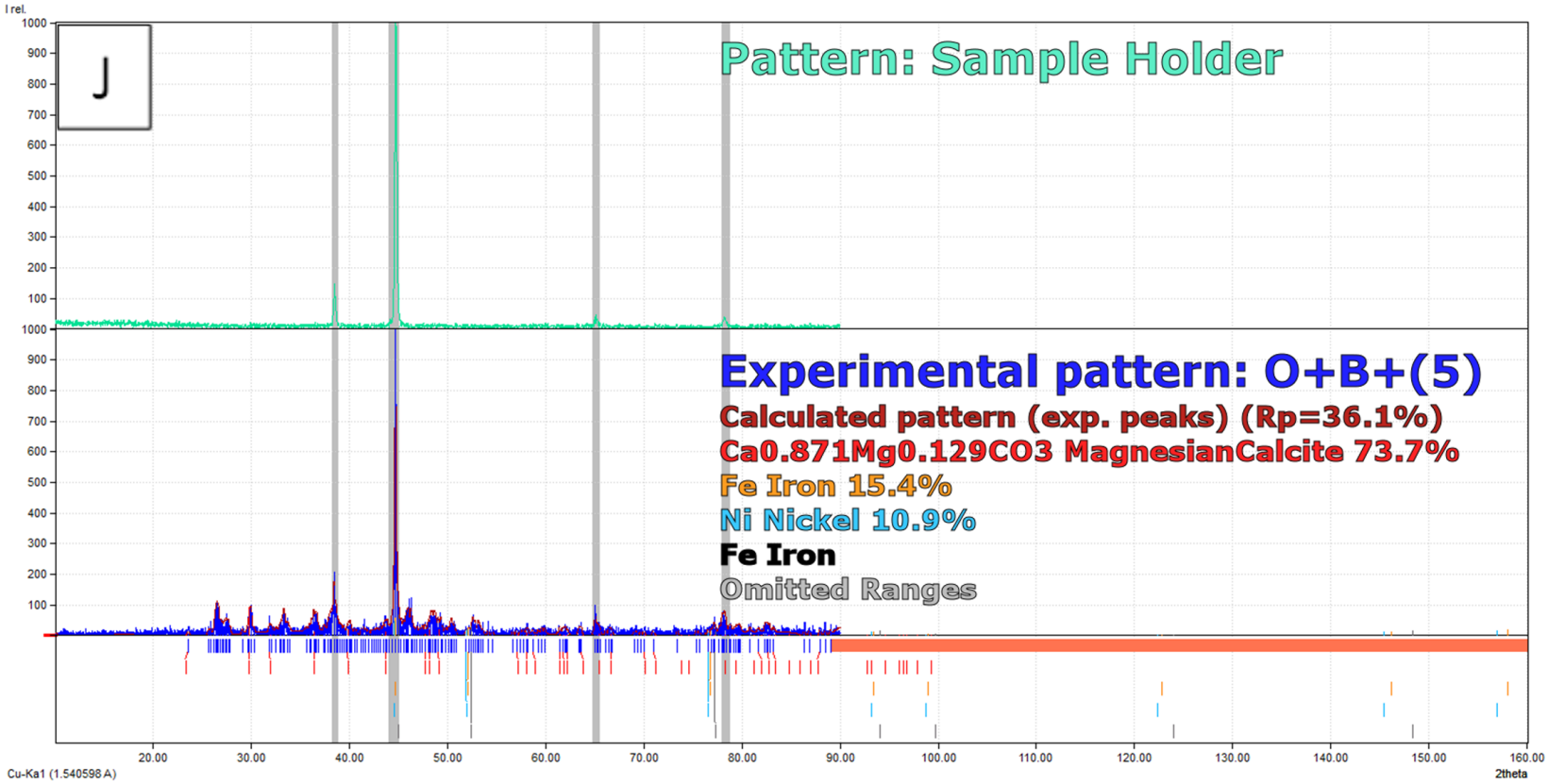
I rel.
J
Pattern: Sample Holder
Experimental pattern: O+B+(5)
Calculated pattern (exp. peaks) (Rp=36.1%)
Ca0.871Mg0.129CO3 MagnesianCalcite 73.7%
Fe Iron 15.4%
Ni Nickel 10.9%
Fe Iron
Omitted Ranges
Cu-Ka1 (1.540598 A)
2theta

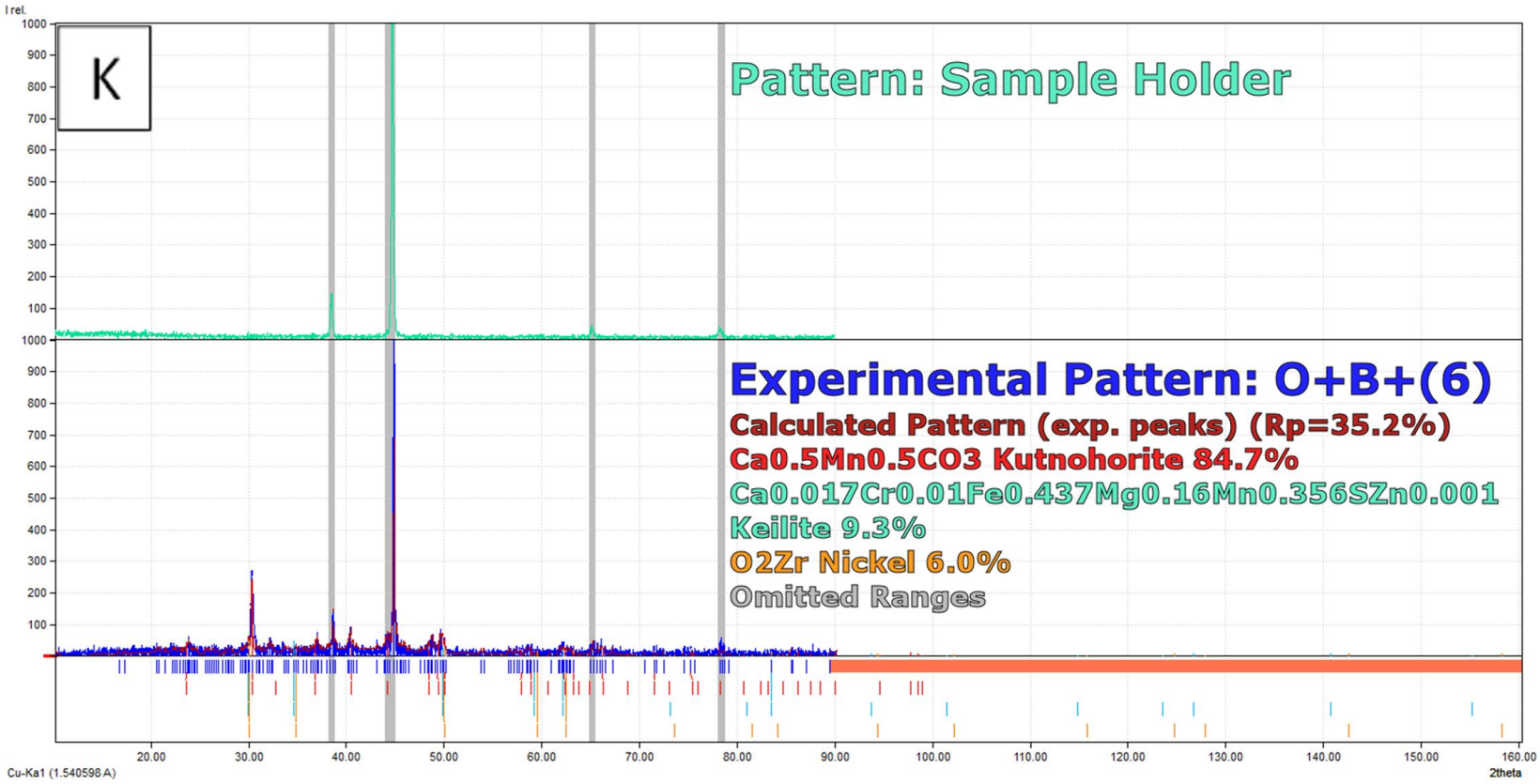
I rel.
K
Pattern: Sample Holder
Experimental Pattern: O+B+(6)
Calculated Pattern (exp. peaks) (Rp=35.2%)
Ca0.5Mn0.5CO3 Kutnohorite 84.7%
Ca0.017Cr0.01Fe0.437Mg0.16Mn0.356SZn0.001
Keilite 9.3%
O2Zr Nickel 6.0%
Omitted Ranges
Cu-Ka1 (1.540598 A)
2theta

References

Aloisi, G., Gloter, A., Krüger, M., Wallmann, K., Guyot, F., and Zuddas, P., 2007, Nucleation of calcium carbonate on bacterial nanoglobules. Geology, v. 34, p. 1017-1020

Anthony, J., Bideaux, R., Bladh, K., and Nichols, M., 2003, Handbook of Mineralogy, Mineralogical Society of America, Chantilly, VA 20151-1110, USA. http://www.handbookofmineralogy.org/

Bizzarro, M., Paton, C., Larson, K., Schiller, M., Trinquier, A., and Ulfbeck, D., 2011, High-precision Mg-isotope measurements of terrestrial and extraterrestrial material by HR-MC-ICPMS-implications for the relative and absolute Mg-isotope composition of bulk silicate Earth. Journal of Analytical Atomic Spectrometry, v.26, p. 565-577

Buczynski, C., and Chafetz, H., 1991, Habit of bacterially induced precipitates of calcium carbonate and the influence of medium viscosity on mineralogy. Journal of Sedimentary Petrology, v. 61, No. 2, p. 226-233

Bundeleva, I. A., Shirokova, L. S., Bénézeth, P., Pokrovsky, O. S., Kompantseva, and E. I., Balor, S., 2012, Calcium carbonate precipitation by anoxygenic phototrophic bacteria. Chemical Geology, v. 291, p. 116-131

Chafetz, H. S., Rush, P. F., and Utech, N. M., 1991, Microenvironmental controls on mineralogy and habit of $CaCO_3$ precipitates: an example from an active travertine system. Sedimentology. v. 38(1), p. 107-126

Chafetz, H. S., and Buczynski, C., 1992, Bacterially induced lithification of microbial mats. Palaios, v. 7, p. 277-293

Chang, V.T., Williams, R., Makishima, A., Belshawl, N.S., and O'Nions, R.K., 2003, Purification of Mg from low-Mg biogenic carbonates for isotope ratio determination using multiple collector ICP-MS. Journal of Analytical Atomic Spectrometry, v.18, p.296-301

Chang, V.T., Williams, R., Makishima, A., Belshawl. N.S., O'Nions, R.K., 2004, Mg and Ca isotope fractionation during CaCO3 biomineralisation. Biochemical and Biophysical Research Communications v. 323(1) , p. 79-85.

De Yoreo, J. J., and Vekilov, P. G., 2003, Principles of crystal nucleation and growth. Reviews in Mineralogy and Geochemistry, v. 54(1), p. 57-93

Downs, R. T. and Hall-Wallace, M., 2003, The American Mineralogist Crystal Structure Database. American Mineralogist 88, 247-250. p.277-293

Dupraz, C., Reid, R. P., Braissant, O., Decho, A., Norman, R. S., and Visscher, P. T., 2009, Processes of carbonate precipitation in modern microbial mats. Earth-Science Reviews, v. 96 (3), p. 141-162

Ehrlich, H.L., 2002, Geomicrobiology 4th edition. Marcel Dekker, Inc., New York, p. 193-194

Farquhar, J., Bao, H., Thiemens, M., 2000, Atmospheric influence of Earth's earliest sulfur cycle. Science, v. 289 (5480), p. 756–758

Folk, R. L., 1974, The natural history of crystalline calcium carbonate: effect of magnesium content and salinity. Journal of Sedimentary Research, v. 44(1), p. 40-53

Gagnon, A.C., DePaolo, D.J., and DeYoreo, J.J., 2010, Calcium isotope signature of amorphous calcium carbonate: a probe of crystallization pathway?. AGU Fall Meeting Abstracts

Galy, A., Bar-Matthews, M., Halicz, L., and O'Nions, R., 2002, Mg isotopic composition of carbonate: insight from speleothem formation. Earth and Planetary Science Letters, v. 201, p. 105-115

Galy, A., Yoffe, O., Janney, P.E., Williams, R.W., Cloquet, C., Alard, O., Halicz, L., Wadwha, M., Hutcheon, I.D., Ramon, E., and Carignan, J., 2003, Magnesium isotopes heterogeneity of the isotopic standard SRM980 and new reference materials for magnesium-isotope-ratio measurements. Journal of Analytical Atomic Spectrometry v. 18, p. 1352-1356

Given, R.K., and Wilkinson, B.H., 1985, Kinetic control of morphology, composition, and mineralogy of abiotic sedimentary carbonates. Journal of Sedimentary Petrology, v. 55, p. 109-119

Giuffre, A., 2015, Biomolecular Controls on Calcium Carbonate Formation by Amorphous and Classical Pathways: Insights from Measurements of Nucleation Rates and Isotope Tracers. PhD dissertation, Virginia Polytechnic Institute and State University

Grazulis, S., Chateigner, D., Downs, R. T., Yokochi, A. T., Quiros, M., Lutterotti, L., Manakova, E., Butkus, J., Moeck, P. and Le Bail, A., 2009, Crystallography Open Database – an open-access collection of crystal structures. Journal of Applied Crystallography, v. 42, p. 726-729

Gražulis, S., Daškevič, A., Merkys, A., Chateigner, D., Lutterotti, L., Quirós, M., Serebryanaya, N. R., Moeck, P., Downs, R. T. and LeBail, A., 2012, Crystallography Open Database (COD): an open-access collection of crystal structures and platform for world-wide collaboration. Nucleic Acids Research v. 40 (D1), p. D420-D427

Gunkel, W., and Rheinheimer, G., 1968, Baktierien: in C. Schlieper. Jena, ed., Methoden der Meeresbiologischen Forschung, VEB Fischer, p. 142-157and p.243-255 (from Krumbein, 1971)

Hammes, F., Boon, N., Villiers, J., Verstraete, W., and Siciliano, S.D., 2003, Strain-specific ureolytic microbial carbonate precipitation. Applied and Evironmental Micro Biology, v. 69, p. 4901-4909

Heidenreich, J. E., and Thiemens, M. H., 1986, A non-mass-dependent oxygen isotope effect in the production of ozone from molecular oxygen: the role of molecular symmetry in isotope chemistry. The Journal of Chemical Physics, v. 84 (4), p. 2129

Hem, J.D., 1985. Study and Interpretation of the Chemical Characteristics of Natural Water. United States Government Printing Office, Virginia.

Hippler, D., Buhl, D., Witbaard, R., Richter, D. K., and Immenhauser, A., 2009, Towards a better understanding of magnesium-isotope ratios from marine skeletal carbonates. Geochemica et Cosmochimica Acta, v. 73, p. 6134-6146

Immenhauser, A., Buhl, D., Richter, D., Niedermayr, A., Riechelmann, D., Dietzel, M., and Schulte, U., 2010, Magnesium-isotope fractionation during low-Mg calcite precipitation in a limestone cave – Field study and experiments. Geochemica et Cosmochemica Acta, v. 74, p. 4346-4364

Kendall, C., and McDonnell (Eds.), J. J., 1998, Isotope Tracers in Catchment Hydrology. Elsevier Science B. V., Amsterdam, p. 51-86

Krumbein, W. E., 1971, Sediment microbiology and grain-size distribution, as related to tidal movement, during the first mission of the West German Underwater Laboratory "Helgoland". Marine Biology, v. 10, p. 101-112

Li, W., Chakraborty, S., Beard, B.L., Romanek, C. S., and Johnson, C. M., 2012, Magnesium isotope fractionation during precipitation of inorganic calcite under laboratory conditions. Earth and Planetary Science Letters, v. 333 – 334

MARLAP, 2004, Multi-Agency Radiological Laboratory Analytical Protocols Manual. Washington, DC, Chapter 14, p. 59-72

Martinez, R. E., Pokrovsky, O. S., Schott, J., and Oelkers, E. H., 2008, Surface charge and zeta-potential of metabolically active and dead cyanobacteria. Journal of Colloid and Interface Science, v. 323, p. 317-325

Mavromatis, V., Pearce, C. R., Shirokova, L. S., Bundeleva, I. A., Pokrovsky, O. S., Benezeth, P., and Oelkers, E. H., 2012, Magnesium isotope fractionation during hydrous magnesium carbonate precipitation with and without cyanobacteria. Geochemica et Cosmochemica Acta, v. 76, p. 161-174

Mavromatis, V., Gautier, Q., Bosc, O., and Schott, J., 2013, Kinetics of Mg partition and Mg stable isotope fractionation during its incorporation in calcite. Geochimica et Cosmochimica Acta, v. 114, p. 188-203

Merino, A., Ginés, J., Tuccimei, P., Soligo, M., and Fornós, J.J., 2014, Speleothems in Cova des Pas de Vallgornera: their distribution and characteristics within an extensive coastal cave from the eogenetic karst of southern Mallorca (Western Mediterranean). International Journal of Speleology, v. 43 (2), p. 125-142

Morita, Y., 1980, Calcite precipitation by marine bacteria. Geomicrobiology Journal, v. 2, no. 1, p. 63-82

Morse, J., and Mackenzie, F., 1990, Geochemistry of Sedimentary Carbonates. Elsevier, Amsterdam

Morse, J., Wang, Q., and Tsio, M., 1997, Influences of temperature and Mg/Ca ratio on $CaCO_3$ precipitates from seawater. Geology, v.25, no. 1, p. 85-87

Nielsen, L.C., DePaolo, D.J., De Yoreo, J.J., 2012, Self-consistent ion-by-ion growth model for kinetic isotopic fractionation during calcite precipitation. Geochimica et Cosmochimica Acta, v 86, p. 166-181

Obst, M., Dynes, J.J., Lawrence, J.R., Swerhone, G.D.W., Benzerara, K., Karunakaran, C., Kaznatcheev, K., Tyliszczak, T., and Hitchcock, A.P., 2009, Precipitation of amorphous $CaCO_3$ (aragoniteilike) by cyanobacteria: A STXM study of the influence of EPS on the nucleation process. Geochemica et Cosmochimica Acta, v. 73, p. 4180-4198

Pogge von Strandmann, P., 2008, Precise magnesium isotope measurements in core top planktic and benthic foraminifera. Geochemistry Geophysics Geosystems, v. 9, no. 12

Railsback, L.B., 2006. Some Fundamentals of Mineralogy and Geochemistry. http://www.gly.uga.edu/railsback/FundamentalsIndex.html

Raz, S., Weiner, S., and Addadi, L., 2000, Formation of high-magnesian calcites via an amorphous precursor phase: possible biological implications. Advanced Materials, v. 12, p. 38-42

Saenger C and Wang Z. 2014. Magnesium isotope fractionation in biogenic and abiogenic carbonates: Implications for paleoenvironmental proxies. Quaternary Science Reviews, v. 90, p. 1-21

Saulnier, S., Rollion-Bard, C., Vigier, N., and Chaussidon, M., 2012, Mg isotope fractionation during calcite precipitation: An experimental study. Geochimica et Cosmochimica Acta, v. 91, p.75-91

Shirokova, L. S., Mavromatis, V., Bundeleva, I. A., Pokrovsky, O. S., Bénézeth, P., Gérard, E., Pearce, C. R., and Oelker, E. H., 2013, Using Mg isotopes to trace cyanobacterially mediated magnesium carbonate precipitation in alkaline lakes. Aquatic Geochemistry, v. 19, p. 1-24

Stephenson, A., Hunter, J., Han, N., DeYoreo, J., and Dove, P., 2011, Effect of ionic strength on the Mg content of calcite: Toward a physical basis for minor element uptake during step growth. Geochimica et Cosmochimica Acta, v. 75, p. 4340-4350

Teng, F-Z., Wadhwa, M., and Helz, R. T., 2007, Investigation of magnesium isotope fractionation during basalt differentiation: Implications for a chondritic composition of the terrestrial mantle. Earth and Planetary Science Letters, v. 261, p. 84-92

Teng, H. H., Dove, P. M., and De Yoreo, J. J., 2000, Kinetics of calcite growth: surface processes and relationships to macroscopic rate laws. Geochimica et Cosmochimica Acta, v. 64(13), p. 2255-2266.

Wang, Z., Hu, P., Gaetani, G., Liu, C., Saenger, C., Cohen, A., and Hart, S., 2013a, Experimental calibration of Mg isotope fractionation between aragonite and seawater. Geochimica et Cosmochimica Acta, v. 102, p. 113-123

Watson, E., 2004, A conceptual model for near-surface kinetic controls on the trace-element and stable isotope composition of abiogenic calcite crystals. Geochimica et Cosmochimica Acta, v.68, p. 1473–1488.

Westall, F., Steele, A., Toporski, J., Walsh, M., Carlton, A., Guidry, S., McKay, D., Gibson, E., and Chafetz, H., 2000, Polymeric substances and biofilms as biomarkers in terrestrial materials: implications for extraterrestrial samples. Journal of Geophysical Research: Planets, v. 105, p. 24511–24527

Wells, A. W., 1971, Cave calcite. Studies in Speleology. v. 2, p. 129-148.

Wombacher, F., Eisenhaur, A., Heuser, A., and Weyer, S., 2009, Separation of Mg, Ca, and Fe from geological reference materials for stable isotope analyses by MC-ICP-MS and double –spike TIMS. Journal of Analytical Atomic Spectrometry, v. 24, p. 627-636

Wombacher, F., Eisenhauer, A., Böhm, F., Gussone, N., Regenbrg, M., Dullo, W. –Chr., and Rüggeberg, A., 2011, Magnesium stable isotope fractionation in marine biogenic calcite and aragonite. Geochemica et Cosmochimica Acta, v. 75, p. 5797-5818

Young E. D. and Galy A., 2004, The isotope geochemistry and cosmochemistry of magnesium. Geochemistry of non-traditional isotopes (eds. C. M. Johnson, B. L. Beard and F.Albare`de). Reviews in Mineralogy and Geochemistry v. 55, p. 197–230.

ZoBell, C. E., 1941, Studies on marine bacteria. I. The cultural requirements of heterotrophic aerobes. Journal of Marine Research, v. 4, p. 42-75

Zuddas, P., and Mucci, A., 1998, Kinetics of calcite precipitation from seawater: II. The influence of ionic strength. Geochimina et Cosmochimica Acta, v. 62, no. 5, p. 757-766